ESA Climate Change Initiative – Fire_cci

D4.1 Product Validation and Intercomparison Report (PVIR)

Project Name	ECV Fire Disturbance: Fire_cci
Contract Nº	4000126706/19/I-NB
Issue Date	15/10/2020
Version	1.1
Author	Daniela Stroppiana, Mirco Boschetti, Lorenzo Busetto, Corrado Luini, Matteo Sali, Magín Franquesa, Joshua Lizundia-Loiola
Document Ref.	Fire_cci_D4.1_PVIR_v1.1
Document type	Public

To be cited as: Stroppiana D., Boschetti M., Busetto L., Luini C., Sali M., Franquesa M. Lizundia-Loiola J. (2020) ESA CCI ECV Fire Disturbance: D4.1 Product Validation and Intercomparison Report, version 1.1. Available at: https://climate.esa.int/en/projects/fire/key-documents/

Project Partners

Prime Contractor/ Scientific Lead & Project Management	UAH – University of Alcala (Spain)
Earth Observation Team	UAH – University of Alcala (Spain) UPM – Universidad Politécnica de Madrid (Spain) CNR-IREA - National Research Council of Italy – Institute for Electromagnetic Sensing of the Environment (Italy)
System Engineering	BC – Brockmann Consult (Germany)
Climate Modelling Group	MPIM – Max Planck Institute for Meteorology (Germany) CNRS - National Centre for Scientific (France)

Distribution

Affiliation	Name	Address	Copies
ESA	Clément Albergel (ESA)	clement.albergel@esa.int	electronic copy
Project Team	Emilio Chuvieco (UAH) M. Lucrecia Pettinari (UAH) Joshua Lizundia-Loiola (UAH) Gonzalo Otón (UAH) Mihai Tanase (UAH) Consuelo Gonzalo (UPM) Dionisio Rodríguez Esparragón (UPM) Daniela Stroppiana (IREA) Mirco Boschetti (IREA) Thomas Storm (BC) Angelika Heil (MPIM) Idir Bouarar (MPIM) Florent Mouillot (LSCE) Philippe Ciais (LSCE)	emilio.chuvieco@uah.es mlucrecia.pettinari@uah.es joshua.lizundia@uah.es gonzalo.oton@uah.es mihai.tanase@uah.es consuelo.gonzalo@upm.es dionisio.rodriguez@ulpgc.es stroppiana.d@irea.cnr.it boschetti.m@irea.cnr.it thomas.storm@brockmann-consult.de angelika.heil@mpimet.mpg.de idir.bouarar@mpimet.mpg.de florent.mouillot@cefe.cnrs.fr philippe.ciais@lsce.ipsl.fr	electronic copy

Summary

This Product Validation and Intercomparison Report (PVIR) describes the implementation of the validation methods and preliminary results derived for assessing the accuracy of global, regional and local BA products, and presents an intercomparison between the FireCCI51 product and other existing global burned area products.

	Affiliation/Function	Name	Date
Prepared	CNR UAH	Daniela Stroppiana Mirco Boschetti Lorenzo Busetto Corrado Luini Matteo Sali Magín Franquesa Joshua Lizundia-Loiola	08/10/2020
Reviewed	UAH	M. Lucrecia Pettinari Emilio Chuvieco	15/10/2020
Authorized	UAH	Emilio Chuvieco	15/10/2020
Accepted	ESA	Clément Albergel	21/10/2020

This document is not signed. It is provided as an electronic copy.

Document Status Sheet

Issue	Date	Details
1.0	31/07/2020	First release of the document
1.1	15/10/2020	Addressing comments of RID of 24/08/2020

Document Change Record

Issue	Date	Request	Location	Details
1.1	15/10/2020	ESA	Executive summary Sections 2.1, 2.3.3.1, 2.3.3.2 Section 2.2 Section 2.3 Section 2.3.1 Section 2.3.1.2 Section 2.3.2 Section 3.2	Minor grammar changes Sections updated Last paragraph updated Figure 2 updated Caption of figure 3 updated Minor changes in the text Minor changes in the text and Figure 11 updated Figure 39 updated

Table of Contents

List of Tables

List of Figures

1 Executive Summary

The Product Validation and Intercomparison Report (PVIR) describes methods and preliminary results of tasks carried out for assessing the quality of burned area (BA) global and regional products derived by applying Fire_cci algorithms. In particular, the global **FireCCI51**, continental **FireCCISFD20** and regional **FireCCIS1S2AF10** BA products are object of this document.

In order to assess the accuracy of the above-mentioned BA products, fire reference perimeters are derived from Earth Observation (EO) data at higher spatial resolution, when available. Validation of global and continental BA products requires systematic sampling of validation units in order to provide robust statistical metrics; for this reason, the most suitable sources of data for deriving reference fire perimeters are Landsat 8 (L8) and Sentinel-2 (S2) for global and regional/continental products, respectively.

A separate case is the validation of BA products over test sites in Africa where a Sentinel-1 (S1) plus S2 algorithm is being developed and tested. In this case, Planetscope data at 3 m spatial resolution are used to assess algorithm performance.

The current report presents the results of the identification of validation units for L8 and S2 EO source data and preliminary results of accuracy metrics of the global **FireCCI51** product for the year 2018.

Complementary, the report also presents an inter-comparison of **FireCCI51** with other existing BA products, more specifically FireCCI41, FireCCI50, FireCCISFD11, and the NASA product MCD64 c6.

2 Validation of Fire_cci products

2.1 Validation protocol

Validation is the assessment of the accuracy of BA products by comparison with reference data/fire perimeters (i.e. ground truth). At global, continental and regional scales, reference data suitable for validation can be extracted primarily from EO data systematically covering the Earth surface; indeed, systematic collection of reliable and representative ground/in situ fire data is hardly feasible to be achieved over large areas.

The major key requirements for reference datasets derived from EO data are i) to be highly accurate and ii) to be generated independently. Independence is a critical characteristic of any validation assessment, since it assures that unbiased accuracies are obtained among products. Independence implies that reference datasets devoted to validation should not be used during the calibration or “tuning” of BA algorithms. EO data with higher spatial resolution compared to the data used for deriving the BA product should be used as long as they provide spatial and temporal systematic coverage of the Earth surface.

Validation of BA products derived from moderate spatial resolution EO data (e.g. MODIS) can be carried out by exploiting data provided by decametric spatial resolution data such as those provided by the Landsat and Sentinel missions (Chuvieco et al., 2018).

In the case of BA products derived from EO data such as Landsat and/or Sentinel (e.g. Roteta et al., 2019, Roy et al., 2019), higher spatial resolution could be provided only by high/very high resolution (HR/VHR) remotely sensed data. Yet this data is characterized by limited temporal and geographical coverage thus not assuring systematic sampling in time and space for the estimation of statistically robust and unbiased accuracy metrics.

Moreover, systematic acquisition of HR/VHR data over large areas might be not easily accessible and/or might have high costs of acquisition. In these cases, satellite images with comparable spatial resolution are commonly used (e.g. Roteta et al., 2019, Roy et al., 2019) and independence is assured by independent processing.

In this framework, and within the Fire_cci project, reference fire perimeters will be mainly built from EO data collected from Landsat and Sentinel missions, which can assure systematic and sufficiently frequent acquisitions over the globe.

For what concerns BA products over the three test sites in Africa, spot acquisitions of HR/VHR EO data could be considered given the limited size of the test areas. This data will complement the validation carried out with medium resolution imagery (mainly Sentinel-2).

Therefore, the protocol implemented for validation of global and regional African BA products is composed of the following steps:

- Identification of validation units: sampling units, which are designed as 100 km by 100 km regions are selected by stratified random sampling in each calendar year, taking into account the major Olson biomes (Olson et al. 2001) and regions with high and low fire intensity/activity as depicted by the FireCCI51 product (Lizundia-Loiola et al., 2020). Specific sampling schemes are adopted for extracting validation units at global and continental scales and based on L8 and S2 acquisition and archive systems, respectively.
- Generation of reference fire perimeters: the area covered by the validation units is subsampled using a 100 km by 100 km window located in the centre of the scene area (i.e. region). Reference fire perimeters over the region are generated from supervised classification of consecutive satellite images, i.e. temporal series of images (L8 for global and S2 for regional Africa). A maximum time step between consecutive images is set to 16/32 days to assure a clear discrimination of the burned surface signal. A 16-day time step is preferred to preserve a clear burned signal of recent burns in those ecosystems where the signal quickly disappears (e.g. tropical savanna, Padilla et al., 2014); however, in ecosystems where the persistence of the burned areas is longer and in presence of frequent cloud cover, the time step could be increased up to 32-days.
- Computation of accuracy metrics: the error matrix (Congalton and Green 1999; Latifovic and Olthof 2004) is extracted by comparing BA products and reference fire perimeters and the following accuracy metrics are computed: commission error ratio, omission error ratio, Dice Coefficient (DC) (Dice 1945), bias and relative bias.

2.2 Validation units: definition

A **validation unit** can be described as a spatio-temporal sampling of the L8/S2 archive used to build temporal series of consecutive scenes suitable for extracting fire reference perimeters.

Spatially the area to be validated (global and continental Africa) is divided into non-overlapping regions to assure equally distributed sampling probability between units. For validating global BA products, the spatial dimension of sampling units will be based on Thiessen Scene Areas (TSAs) constructed over the Landsat WRS-2 by Cohen et al. (2010) and Kennedy et al. (2010) and exploited in previous Fire_cci phases (Padilla et al. 2014;

2015, 2017; Lizundia-Loiola et al., 2020). For validating regional-Africa BA products, the non-overlapping regions are assumed coincident with S2 tiles (see section 2.4.1)

However, compared to previous Fire_cci phases, the region for extracting fire reference perimeters within each unit was increased to 100 km by 100km: hence, the validation unit is a 100 km by 100 km subsample of a L8/S2 scene, centred on the L8 frame or S2 tile.

Temporally, a **short unit** is assumed to be composed of two consecutive cloud free L8/S2 scenes (pairs of images) whereas a **long unit** is composed of more than two consecutive pairs (consecutive short units) (Figure 1). Notice that time between consecutive images is set a-priori but does not necessarily coincide with theoretical data acquisition frequency of the satellite mission (L8 and/or S2); hence, the term "consecutive" indicates temporally adjacent images with a preliminarily defined maximum temporal distance.

A L8/S2 scene is assumed to be **cloud free when less than 30% of the land area** within the L8 frame/S2 tile is free of clouds; cloud coverage is retrieved from metadata information associated with L8/S2 Level 2 products.

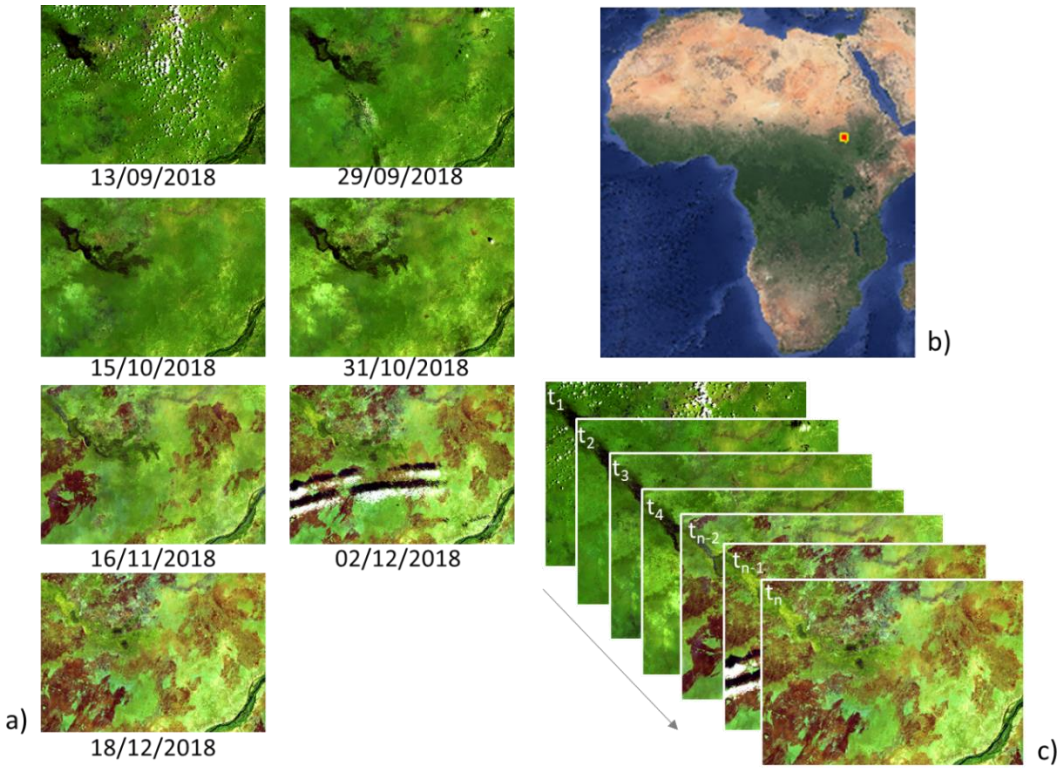

Figure 1: Example of short and long validation units for Landsat frame 173/053 a) consecutive scenes available; b) location of the validation unit; and c) long unit composed of conscutive L8 pairs acquired with a 16-day time step between two dates: t_1 and t_n.

The following parameters are therefore defined to identify temporal sampling for validation units:

- **Time step** between consecutive pairs (i.e. short unit) [days]: $\Delta t = t_k - t_{k-1}$
- **Length of the validation unit** (i.e. long unit) [days]: $L = t_n - t_1$

where within the temporal series of L8/S2 images: $t_1$is the acquisition date of the first scene, $t_n$is the acquisition date of the last scene, $t_k$is the acquisition date of any scene

within the unit. Validation unit length (L) is the time between first and last L8/S2 scenes, where the last date is when the temporal series ends due to a time step greater than the maximum time step between images with cloudiness below 30%.

The long validation unit is identified by setting the **maximum time step** (Δt_{max}) and the **minimum unit length** (L_{min}) and, by setting these two parameters, the population of L8/S2 validation units available for sampling within EO data archives can be identified. Ideally a time step Δt_{max}=16 days guarantees the greatest discrimination between burned and unburned surfaces; this condition becomes particularly relevant in those ecosystems where the duration of the post-fire spectral signal is very short (Padilla et al., 2014). Since in case of persistent cloud coverage, a conservative value of Δt_{max}=16 days could significantly reduce the length of the validation unit, greater values (e.g. Δt_{max}=32 days) could be set in those ecosystems where the burn signal persists longer, such as boreal forests (Padilla et al., 2014). Since Δt_{max} and L_{min} significantly influence the number of suitable validation units depending on L8/S2 image availability, a preliminary analysis of L8/S2 archives was carried out to investigate data availability as a function of these two parameters (Δt_{max} and L_{min}).

2.3 Validation of global BA products

In this section, the approach implemented for building reference fire perimeters for validation of Fire_cci BA global products is described in detail; Figure 2 shows the flowchart of all the conducted steps, from the selection of the validation units to the extraction of fire perimeters over the long validation unit.

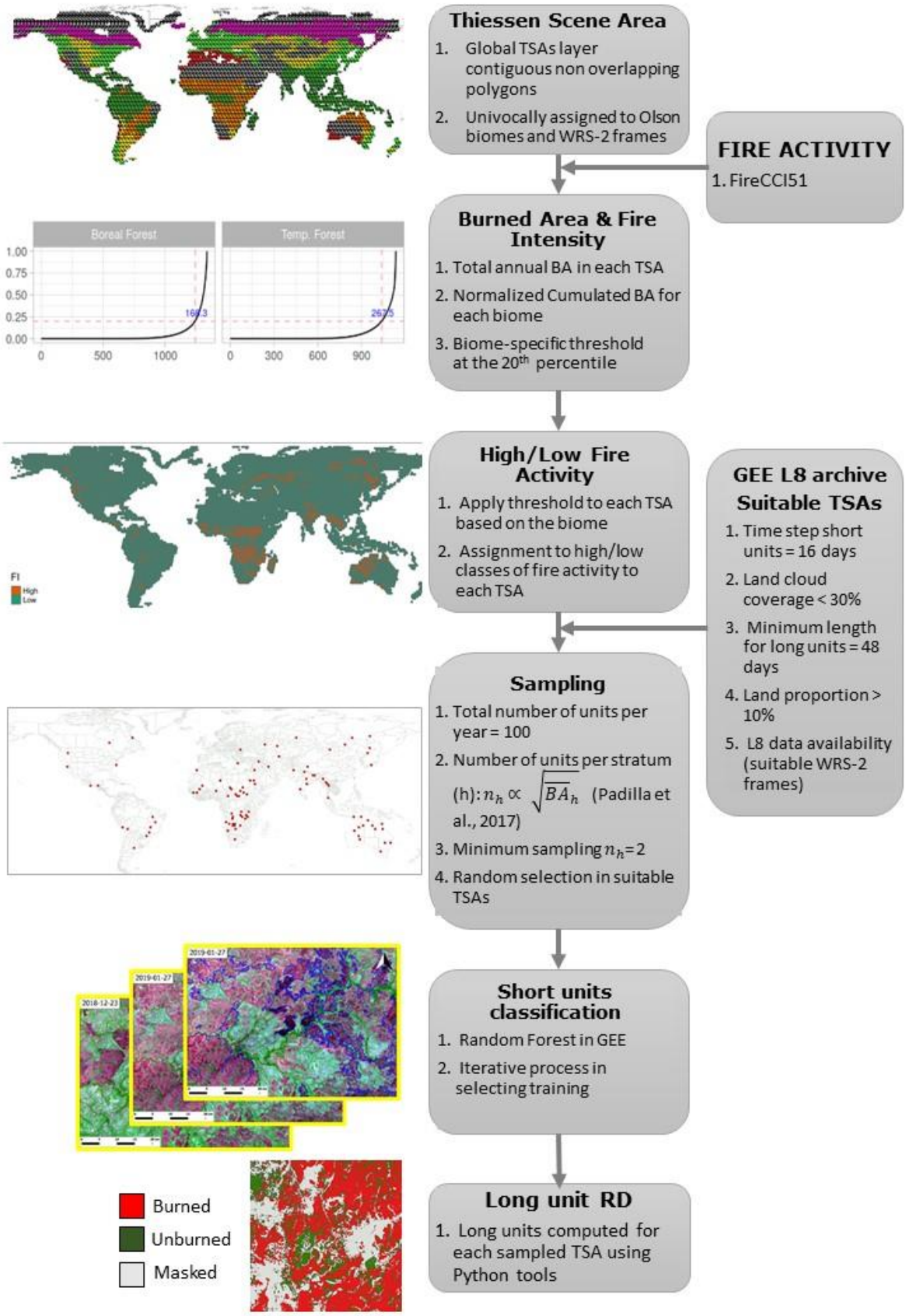

Figure 2: Flowchart of steps for extracting fire reference perimeters for the year 2018 for the global validation: from sampling to classification of the short units and building long units files.

2.3.1 L8 Sampling scheme definition and implementation

Since sampling sites should be selected to properly represent the variety of conditions that affect the accuracy of BA products, both in time and space, a stratified random sampling scheme is adopted. In particular, following Padilla et al. (2017), stratification will be based on i) major Olson biomes (Olson et al. 2001) and ii) areas with high and low fire intensity, as derived within each biome from FireCCI51 BA product (Chuvieco et al., 2018) (Figure 3).

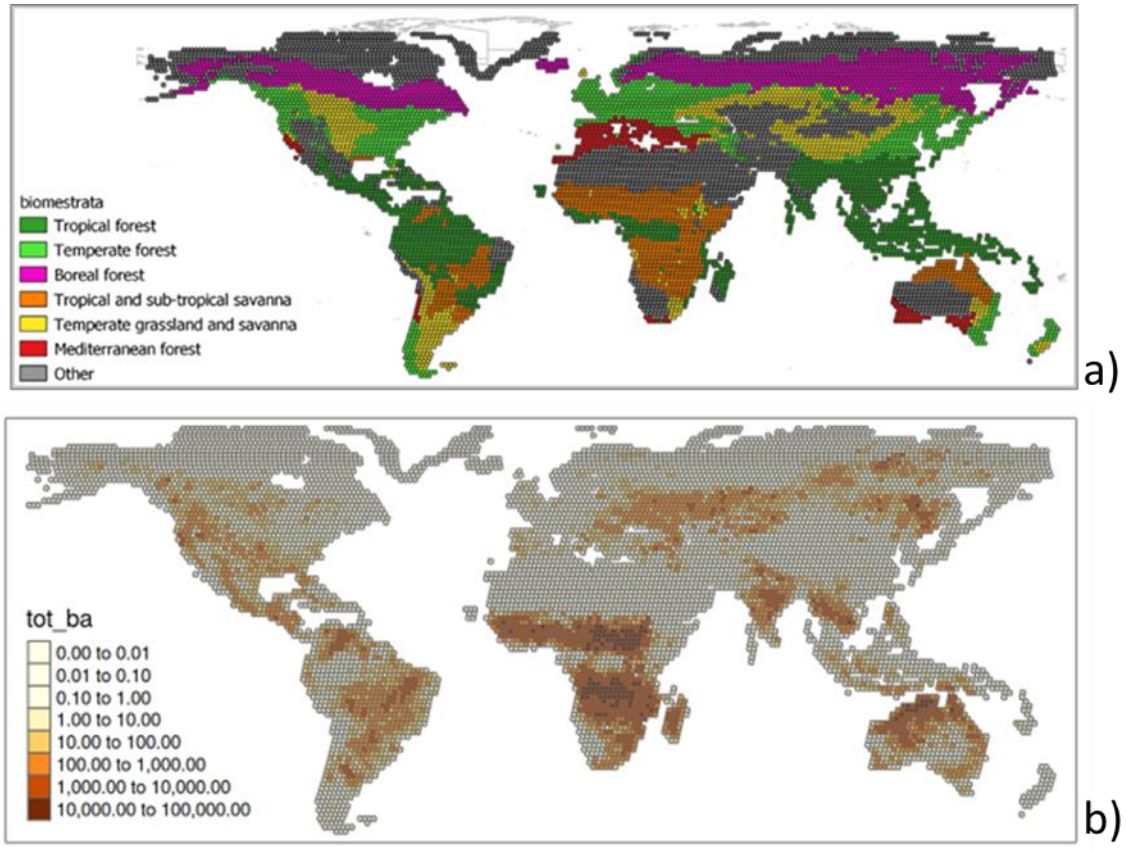

Figure 3: Two layers were used for the definition of the strata in the random stratification sampling: a) Olson biomes (Olson et al. 2001) (top panel), and b) total annual burned area [m2] (i.e. fire intensity) (bottom panel) for the Thiessen scene areas (TSAs) polygons. Fire intensity, quantified by the total annual BA was computed from the 2018 FireCCI51 BA product (Lizundia-Loiola et al., 2020). The class "Other" includes: Tundra, Deserts and Xeric Shrublands, Mangroves.

Specifically, for global BA products, the spatial dimension of sampling units is based on Thiessen Scene Areas (TSAs), as explained in Section 2.2. The number of selected units for each year is equal to 100 TSAs.y^{-1} over the period 2017-2019 (tot = 300).

For each TSA, a long sampling unit is composed of consecutive pairs of Landsat images ("short units"). By doing so, the time period covered by the reference fire perimeters will be sufficiently long to provide a more accurate reporting of the detection of fire date. The use of long units, rather than short units (pairs of L8 images) for extracting reference perimeters, represents an improvement over previous Fire_cci phases. Additionally, for each sampled TSA an area of approximately 100 km by 100 km was selected (i.e. region) for defining reference fire perimeters; with respect to previous Fire_cci, the area has been increased from 20 km x 30 km to allow a more robust analysis of fire size and patches.

2.3.1.1 L8 sampling stratification

As stated above, strata for implementing stratified random sampling of validation units were derived from the intersection of Olson biomes and fire intensity layers. For each TSA, the major Olson biome and high/low fire intensity class were assigned (Figure 3). For each TSA, the amount of burned area is derived from the annual FireCCI51 BA product (Lizundia-Loiola et al., 2020). From year to year, fire area and fire activity might significantly change thus requiring a specific source of information for each considered year to be validated. With respect to previous Fire_cci phases, the source of information for classifying into high/low fire intensity was updated from lower spatial resolution MCD64A1 Version 6 Burned Area data product to the higher resolution FireCCI51 BA product.

In order to assign the high/low fire intensity class, the total annual burned area (TotBA, m^2) was computed in each TSA and these values were then sorted in increasing order; the cumulated sum was computed and normalized with respect to the biome's maximum value of total annual BA. The TotBA value corresponding to the 20th percentile of the normalized cumulated sum (Padilla et al. 2017, Boschetti et al., 2016) provides the threshold for assigning each TSA to either the ***high*** (total annual BA > threshold) or ***low*** (total annual BA <= threshold) fire intensity classes. In Figure 4, the threshold values for each biome for the year 2018 are reported in blue colour; values are also summarized in Table 1.

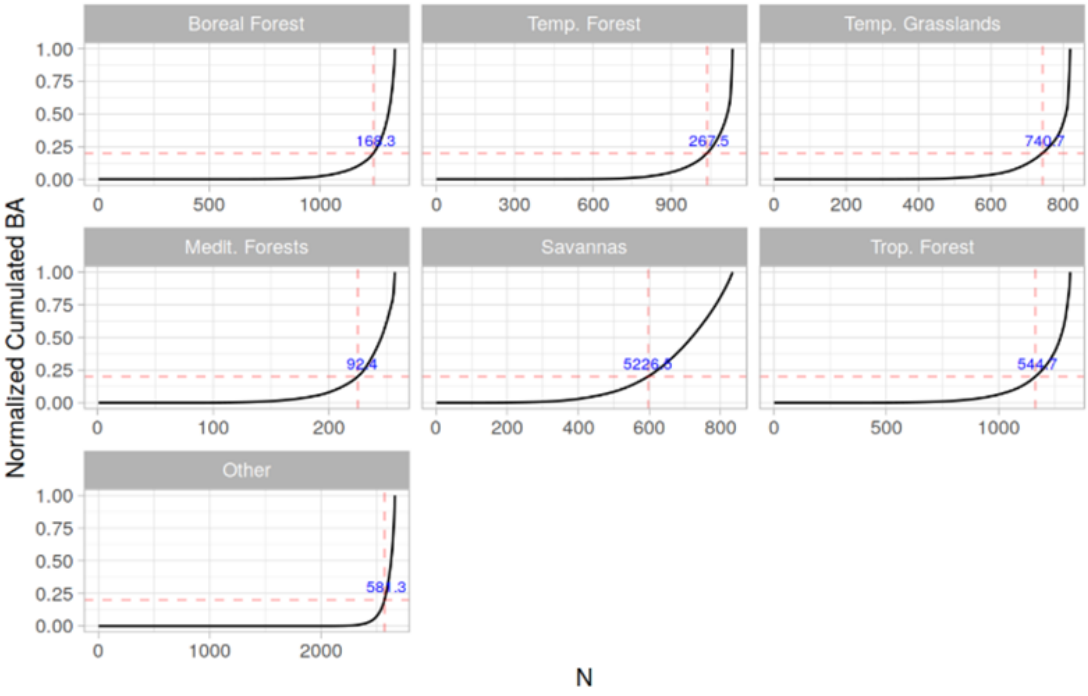

Figure 4: Thiessen scene areas (TSAs) for each biome plotted by increasing normalized total burned area; on the x-axis the increasing cumulated number of TSA (N). Red dashed horizontal line shows the 20th percentile and the corresponding value of total annual burned area used as threshold for assigning high/low fire intensity class.

Table 1. Threshold values identified for further stratification of each biome into high/low fire intensity strata. Threshold values are applied to each TSA for assigning it to either high or low fire intensity class. The number of high and low fire intensity TSAs for each biome and the year 2018 is reported in Table 2.

Biomes	Threshold [km^2]
Boreal Forest	168.3
Mediterranean Forests	92.4
Savannas	5226.5
Temperate Forest	267.5
Temperate Grasslands	740.7
Tropical Forest	544.7
Other	581.3

2.3.1.2 Analysis of L8 data availability 2018

Preliminary analysis of data availability at the global scale was carried out for the year **2018** to investigate the distribution of L8 scenes suitable for sampling. The global L8 archive available in Google Earth Engine (GEE) was investigated to identify, over each validation unit, L8 temporal series **with maximum time step of 16 and/or 32 days between consecutive clear-sky images**.

In this context, L8 images are considered to be "clear-sky" if their cloud coverage percentage is lower than 30%. Information on cloud coverage percentage was extracted from metadata and, specifically, the "Land Cloud Cover" value percentage was used. In order to investigate L8 data availability, the length of the available temporal series (L) over the L8 TSAs was analysed by setting time steps (Δt_{max}) of either 16 or 32 days (see Section 2.2).

Figure 5 and Figure 6 show maximum length and starting month of the long units when Δt_{max}=16 days and Δt_{max}=32 days, respectively. As for previous figures, grey TSAs are those for which no suitable data is available. The figure confirms that Δt_{max} and L are correlated, hence relaxing the condition on maximum time step, from 16 to 32 days, produces longer series (light green and yellow colours).

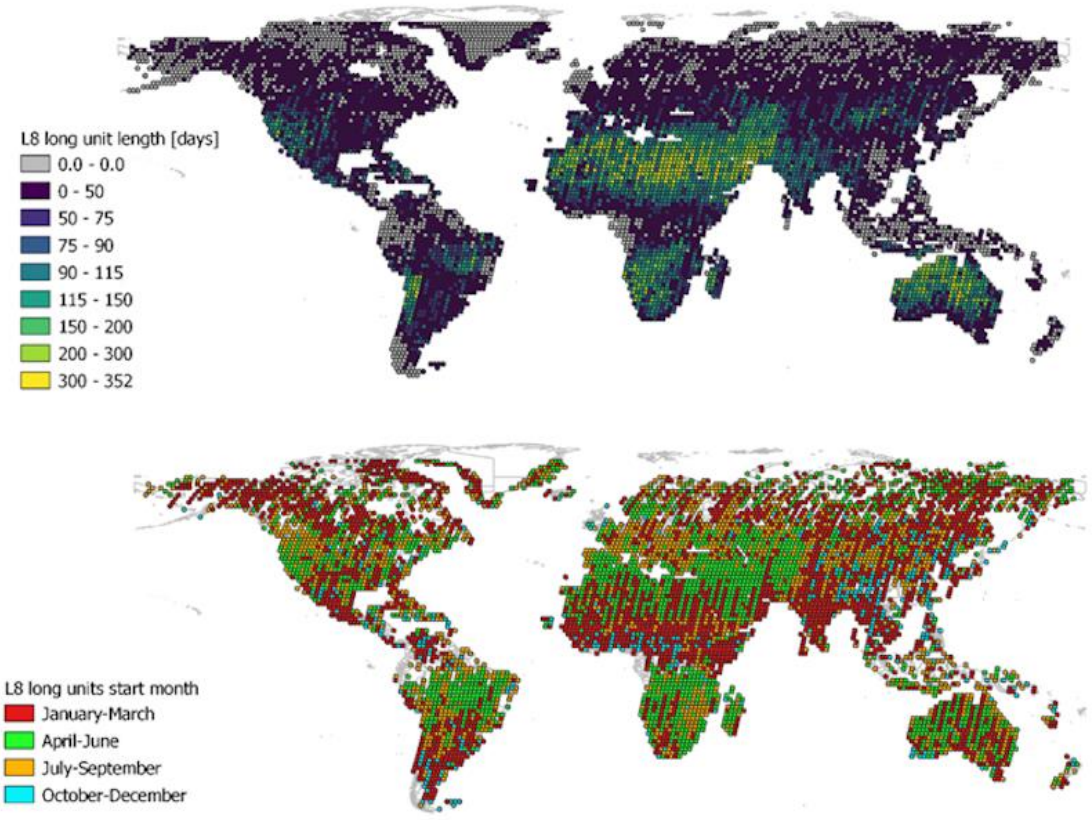

Figure 5: a) Length [days] (top) and starting month (grouped in three-month seasons) (bottom) of the longest temporal series for each TSA (validation unit) with a 16 days maximum time step between consecutive clear sky images.

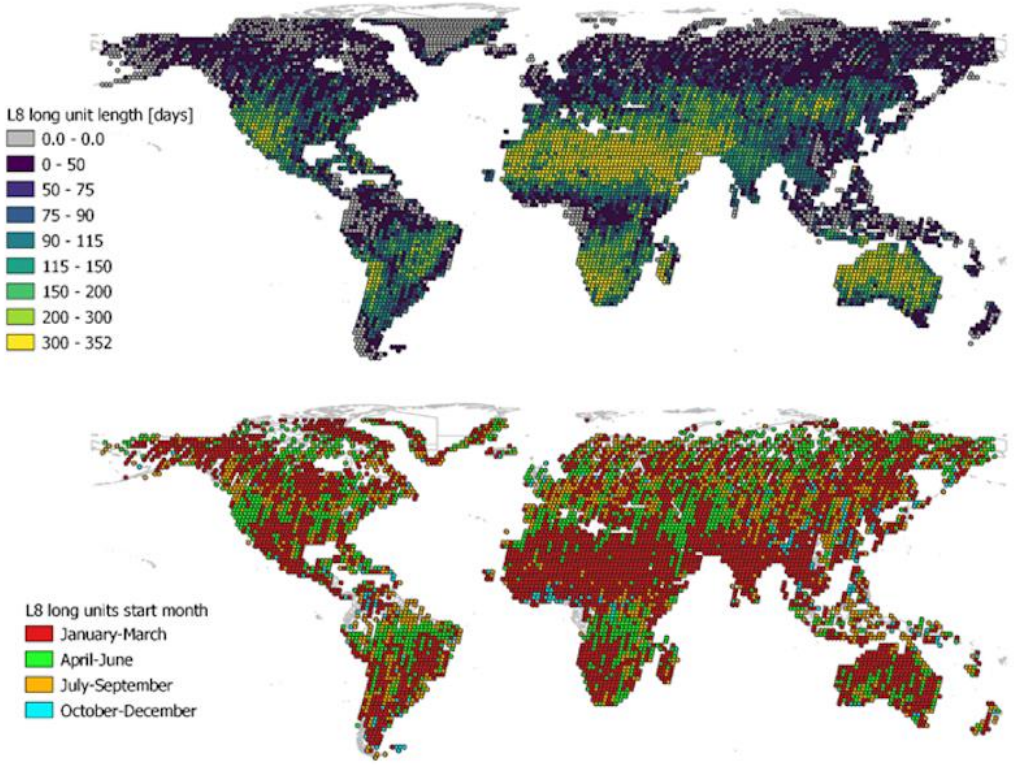

Figure 6: a) Length [days] (top) and starting month (grouped in three-month seasons) (bottom) of the longest temporal series for each TSA (validation unit) with a 32 days maximum time step between consecutive clear sky images.

Figure 7 shows as an example the number and location of available TSAs for each biome with a **maximum time step of 16 days (Δt_{max}=16)** for three values of minimum length (L_{min}): 32, 48 and 112 days. An analysis of the figure highlights that, with the exception of savanna and desert areas (the latter included in the "Other" category), availability of TSAs with length greater than 100 days is limited, in particular when Δt_{max}=16 days. Clearly, increasing the required minimum length of the validation unit, decreases the number of available TSAs for each biome especially for those ecosystems mostly affected by cloud cover (*e.g.* tropical regions). In particular, the number of suitable TSAs significantly decreases when L_{min}=112 days for almost all biomes except savannas (blue regions) thus leading to a spatially bias in TSAs availability.

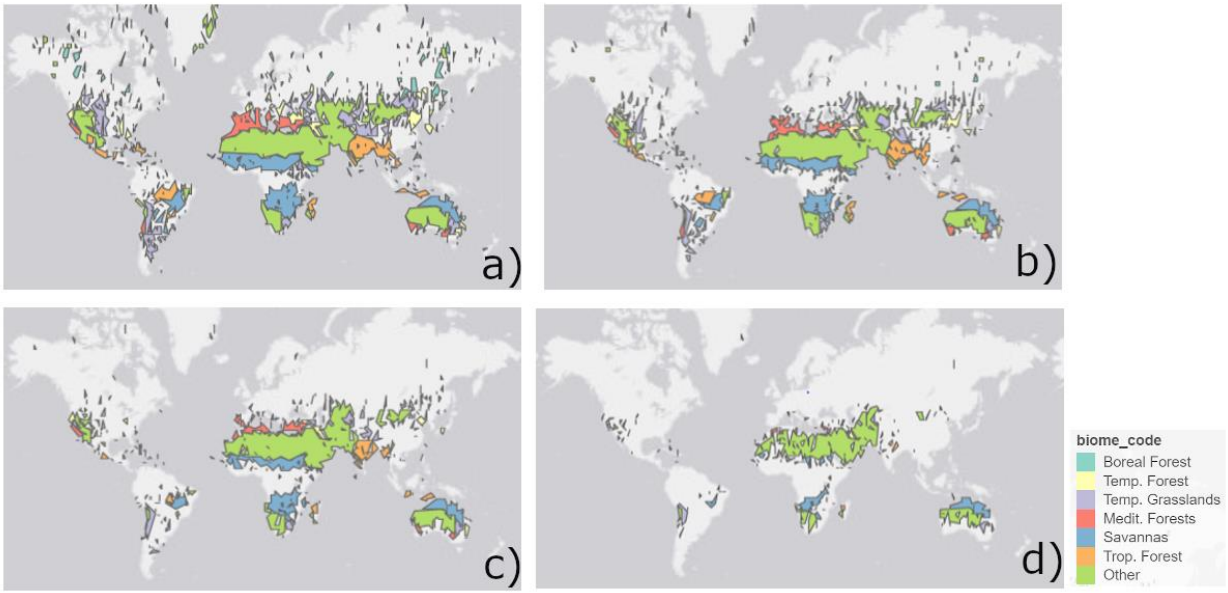

Figure 7: L8 TSAs (validation units) suitable for sampling with a 16 days maximum time step between consecutive scenes and variable total length of the temporal dataset [number of days] for each biome: 32 (a), 48 (b), 64 (c), 112 (d).

This analysis was further carried out by splitting biomes into sub-strata of high/low fire intensity by applying threshold values shown in Table 1. Figure 8 and Figure 9 show the number of TSAs available for sampling as a function of L_{min} (values on top strips) with Δt_{max}=16 days.

Based on the outcome of this analysis, in order to keep a sufficient number and an unbiased global spatial distribution for TSAs of the least represented biomes, the **minimum length of the validation unit was set to 48 days**.

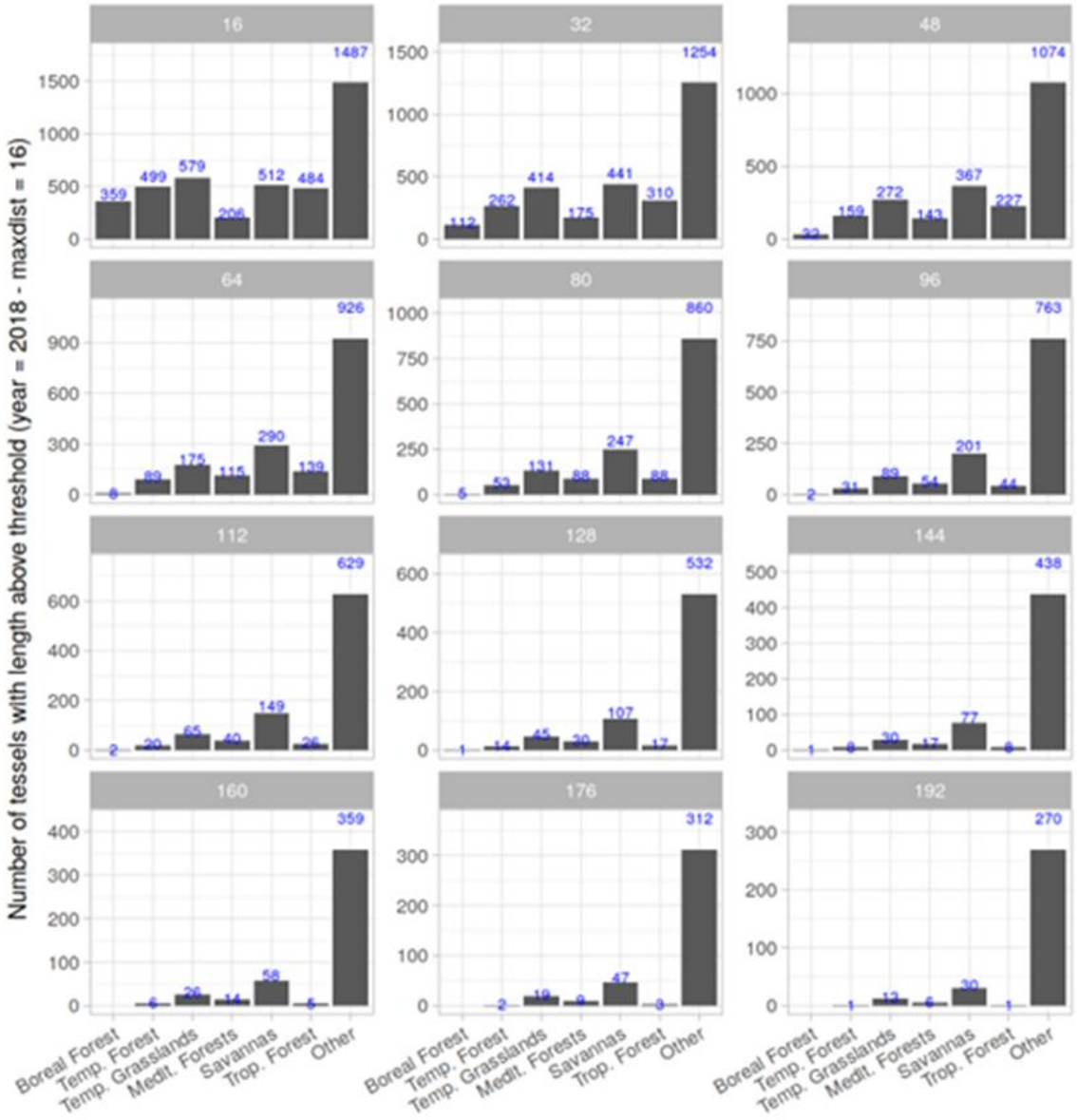

Figure 8: Number of L8 TSAs available for sampling for each biome in the Low Fire Intensity stratum as a function of the length of the minimum temporal dataset/validation unit required (number on top of each panel) with maximum time step set to 16 days.

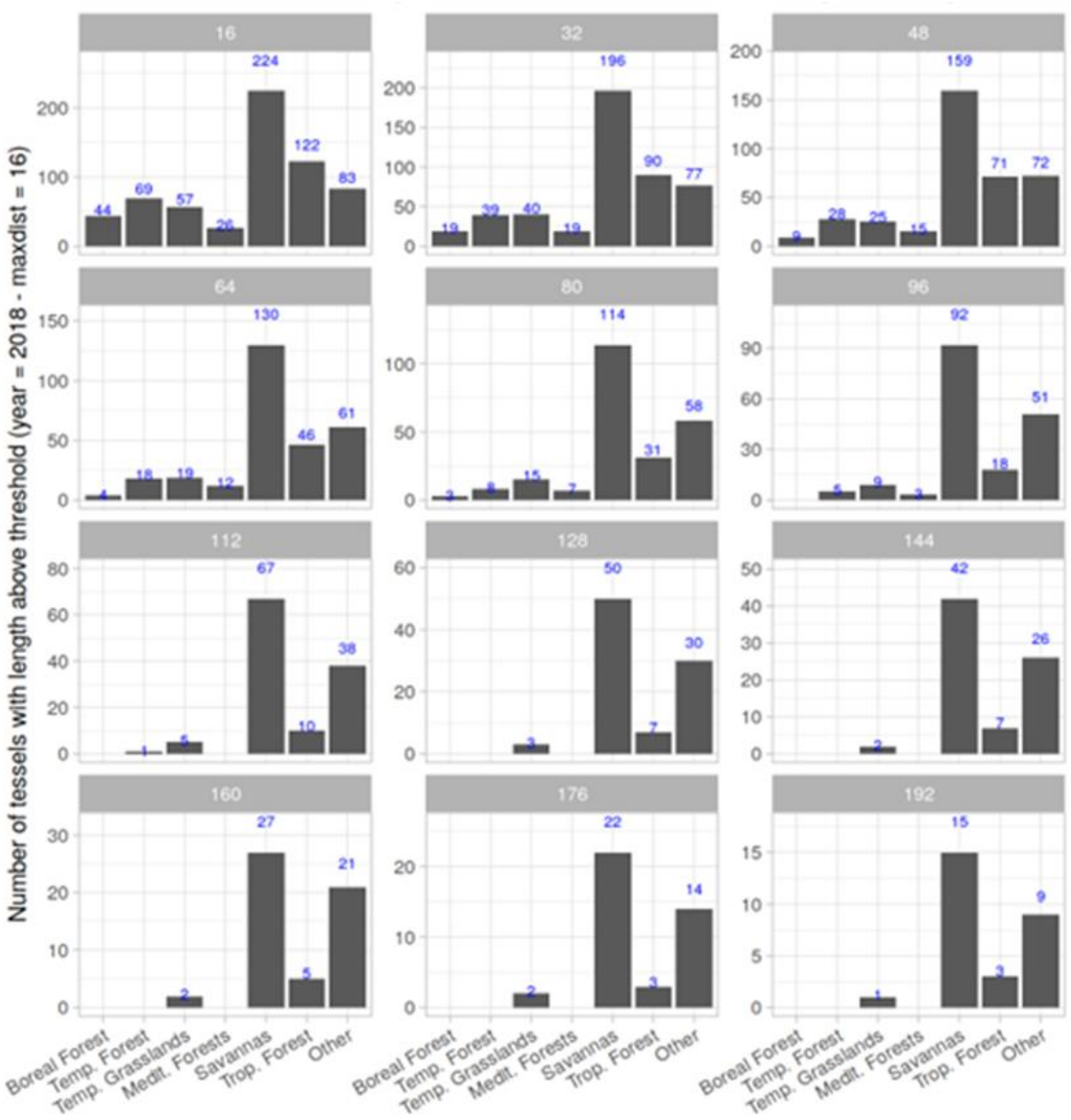

Figure 9: Number of L8 TSAs available for sampling for each biome in the High Fire Intensity stratum as a function of the length of the minimum temporal dataset/validation unit required (number on top of each panel) with maximum time step set to 16 days.

2.3.1.3 Identification of sampling cardinality per stratum

A total of **100 validation** units per year were extracted from the population of available L8 derived with Δt_{max}=16 days and L_{min}=48 days and the total annual number of validation units was distributed among strata based on Eq. 1.

$$n_h \propto N_h \sqrt{\overline{BA}_h} \qquad \text{Eq. 1}$$

where n_h is the number of TSAs to be sampled for each stratum h, $\overline{BA}_h$ is the average total annual burned area for stratum h and N_h is the total amount of TSAs available for sampling for each stratum h. For smaller strata a minimum of n_h= 2 is assigned. Results obtained with this procedure are summarized in Table 2 where for each stratum (combination of biomes and fire intensity) we show the number of TSAs available for sampling and the corresponding number of TSAs to be sampled.

Table 2. Number of TSAs available for sampling in high (N_{HIGH}) and low (N_{LOW}) fire intensity strata, number of sampled TSAs in high (FI_{high}) and low (FI_{low}) fire intensity strata and total number of sampled TSAs for each biome for the year 2018.

Biomes	N_{HIGH}	N_{LOW}	FI_{high}	FI_{low}	Total
Boreal Forest	96	1242	2	4	6
Mediterranean Forests	32	225	2	2	4
Savannas	237	597	23	19	42
Temperate Forest	97	1037	3	5	8
Temperate Grasslands	76	743	5	6	11
Tropical Forest	155	1163	6	10	16
Other	92	2571	4	9	13
Total	**785**	**7578**	**45**	**55**	**100**

A random sampling algorithm is then applied to each stratum to extract the number of validation units shown in Table 2. The location of the sampled TSAs is shown in Figure 10.

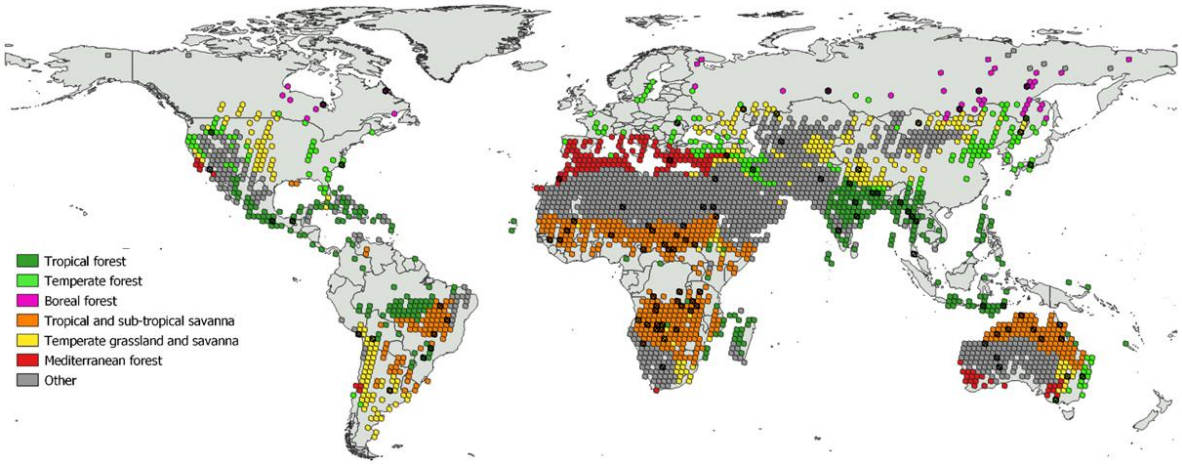

Figure 10: Spatial distribution of the 100 TSAs sampled randomly worldwide (black) for each stratum (biome/fire insentity). Light grey regions show area where not suitable TSAs are available according to criteria outlined in 2.3.1.1.

2.3.2 Extraction of L8 fire reference perimeters

Figure 11 shows the flowchart of the steps for extracting fire perimeters over L8 validation units composed of six major steps (Step 1 to Step 6 in the figure and in the text); input to the processing are L8 short units (consecutive L8 images) to extract areas that burned between the two dates (t_1, t_2). All short units over the same area are combined to derive fire perimeters over the L8 long unit. The steps are described below.

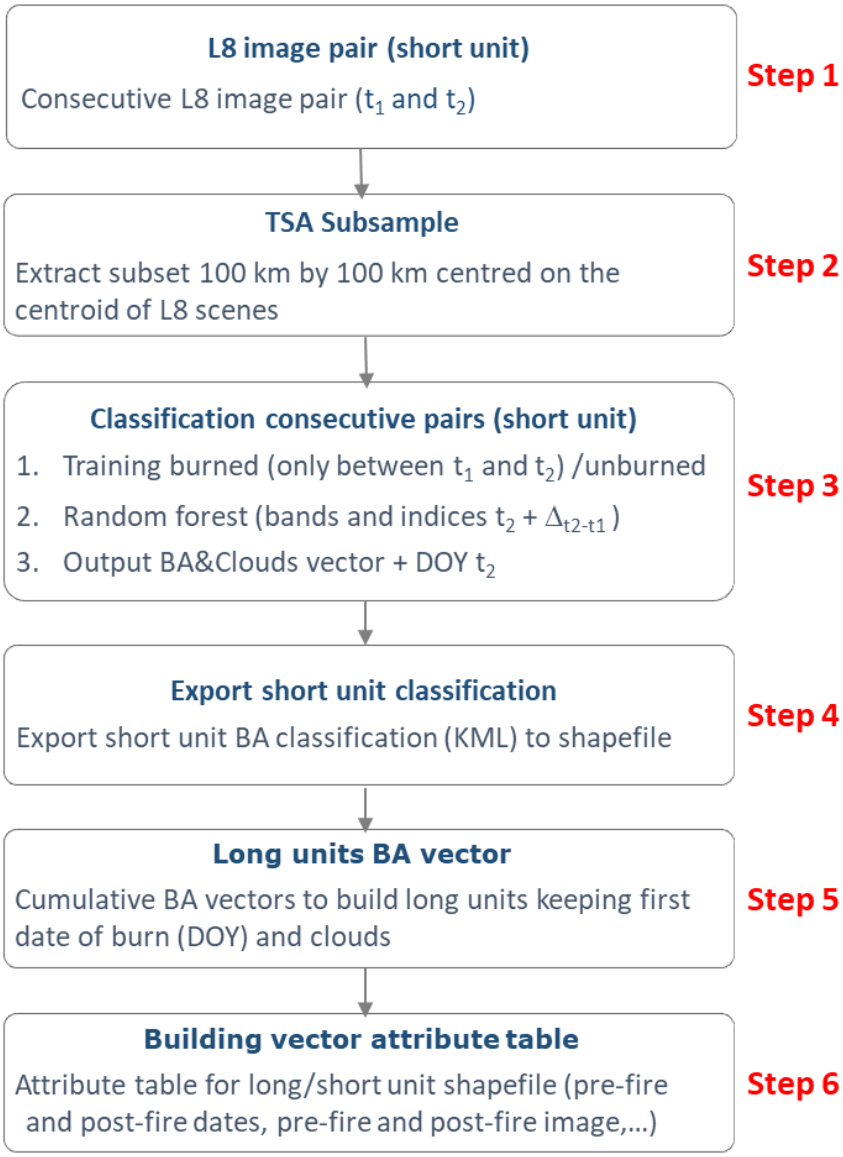

Figure 11: Flowchart showing steps for extraction of fire reference perimeters over sampled TSAs / validation units.

1. **L8 image pair (short unit)**: over each TSA, consecutive L8 scenes (Δt_{max}=16 days) made available as Level 2 product (surface reflectance) with cloud cover layer used for masking not observable pixels.
2. **TSA Subsample**: extraction of validation area of size 100 km by 100 km centred at L8 frame's centroid.
3. **Classification consecutive pairs (short unit)**: extraction of perimeters of the areas that burned between the two dates (t_1, t_2) by applying a Random Forest (RF) algorithm. This step requires the selection of training areas over burned and unburned surfaces carried out in GEE and by visual interpretation of the expert. The RF algorithm is run using all L8 spectral bands and the Normalized Burn Ratio (NBR, Key and Benson 1999), Normalized Burned Ratio 2 (NBR2, Roy et al. 2005) and Normalized Difference Vegetation Index (NDVI, Rouse et al. 1974).
4. **Export short unit classification**: the layer of fire perimeters for the short unit is exported as a KML file; this file contains polygons for burned areas and clouds together with information on burn detection date (t_2 stored as Day of the Year-DOY).

5. **Long Unit BA vector**: all short unit vector files for a specific TSA are stored and converted to shapefile (.shp) and cumulative fire perimeters over the long unit are derived by retaining first date of burn detection for each polygon; in this step, cumulated cloud cover is used for masking those pixels that have been observed as cloudy at least once during the long unit period. That is, only pixels that have been cloud free over the entire time period covered by the long unit are classified into burned/unburned. This step is carried out with a script coded in Arcpy.
6. **Building vector attribute table**: for both short and long units, attribute tables are built containing all information relative to each polygon about pre- (t_1) and post-fire (t_2) dates and L8 scene identifier (Scene ID), detection dates, category (burned, unburned and masked).

The core of the processing of the L8 short units (short unit classification) was implemented in GEE. A script was coded to perimeter existing burned areas between two consecutive images, identified by acquisition dates (Start, End). Input parameters to run the program are:

- L8 frame path/row;
- L8 dataset (the image collection to be filtered)
- Year;
- Starting date (t1);
- Ending date (t2);

The script needs to be run twice. The first time the dataset is filtered by the dates of input images (Pre_Image, Post_Image) and a cloud mask is applied. Then spectral indices NBR, NBR2 and NDVI and temporal differences are computed.

The images are displayed as RGB false colour composites (SWIR2, NIR, Red) and the training regions over burned and unburned areas are defined by the user as vector format. If available, training polygons can be uploaded as asset on the GEE platform.

The script is then run a second time to apply a Random Forest algorithm for classification of burned areas, using the input layers identified above (spectral bands, indices and their temporal difference).

The output layers consist of:

- Burned areas in vector KML format;
- The validation region of 100 km x 100 km obtained by a buffering of the centroid of the L8 frames;
- Cloud Mask in vector format;
- Training polygons in vector format;

The classification of the L8 short units is then converted to shapefile format and processed to extract fire reference perimeters, clouds and burn date.

Figure 12 shows an example fire reference perimeter product extracted from a L8 long validation unit over frame 173/053 (path/row, Africa). Masking cloud areas is necessary to achieve the highest accuracy in the detection on the burn dates; although burned surface and burned signal can be persistent and last over time, the occurrence of clouds over the area might prevent the accurate detection of the burn date. However, since cumulated cloud cover might significantly reduce the total area sampled at the end of the validation period over each TSA, additional criteria are under investigation to combine maximum time step, unit length and cumulated cloud cover. These criteria will be tested for the S2 sampling approach over continental Africa.

Figure 13 shows an example of attribute table for fire reference perimeters over the long unit.

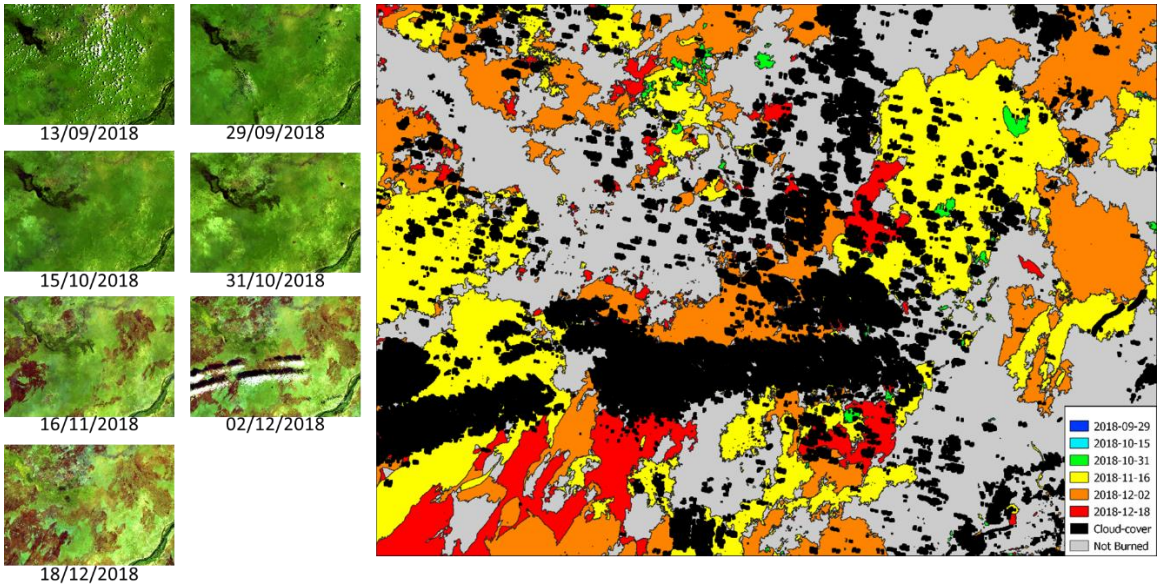

Figure 12: Example of reference fire perimeters extracted over L8 frame 173/053 (Path/Row), Africa; on the left RGB false color composites of the L8 scenes that are part of the validation long unit, in the right the reference burned area perimeters extracted by RF classification with reference to the date of detection (color of the polygons). Black regions are regions masked for cloud cover and grey areas are unburned.

category	preDate	postDate	preImg	postImg	path	row	year	area
3	2018-06-14	2018-10-20	LC81760712018165LGN00	LC81760712018293LGN00	176	71	2018	4139444454,420...
1	2018-10-04	2018-10-20	LC81760712018277LGN00	LC81760712018293LGN00	176	71	2018	291918,1587459...
1	2018-10-04	2018-10-20	LC81760712018277LGN00	LC81760712018293LGN00	176	71	2018	16721,86342880...
1	2018-10-04	2018-10-20	LC81760712018277LGN00	LC81760712018293LGN00	176	71	2018	5400,00000000000
1	2018-10-04	2018-10-20	LC81760712018277LGN00	LC81760712018293LGN00	176	71	2018	193468,5110210...
1	2018-10-04	2018-10-20	LC81760712018277LGN00	LC81760712018293LGN00	176	71	2018	36000,00000000...
1	2018-10-04	2018-10-20	LC81760712018277LGN00	LC81760712018293LGN00	176	71	2018	43026,44852310...
1	2018-10-04	2018-10-20	LC81760712018277LGN00	LC81760712018293LGN00	176	71	2018	24176,49163130...
1	2018-10-04	2018-10-20	LC81760712018277LGN00	LC81760712018293LGN00	176	71	2018	186999,5500189...
1	2018-10-04	2018-10-20	LC81760712018277LGN00	LC81760712018293LGN00	176	71	2018	1609138,969650...
1	2018-10-04	2018-10-20	LC81760712018277LGN00	LC81760712018293LGN00	176	71	2018	71100,00000000...
1	2018-10-04	2018-10-20	LC81760712018277LGN00	LC81760712018293LGN00	176	71	2018	62173,63504820...
1	2018-10-04	2018-10-20	LC81760712018277LGN00	LC81760712018293LGN00	176	71	2018	31500,00000000...
1	2018-10-04	2018-10-20	LC81760712018277LGN00	LC81760712018293LGN00	176	71	2018	6334,84491956000
1	2018-10-04	2018-10-20	LC81760712018277LGN00	LC81760712018293LGN00	176	71	2018	60300,00000000...
1	2018-10-04	2018-10-20	LC81760712018277LGN00	LC81760712018293LGN00	176	71	2018	7243335,088220...
1	2018-10-04	2018-10-20	LC81760712018277LGN00	LC81760712018293LGN00	176	71	2018	1350938,461050...
1	2018-10-04	2018-10-20	LC81760712018277LGN00	LC81760712018293LGN00	176	71	2018	43200,00000000...

Figure 13: Example of the attribute table of a reference fire perimeters shapefile over validation long units: category can be assigned to burned (1), cloud (2) and unburned (3), preDate and postDate are the pre-fire and post-fire dates of the short unit from which the polygon was extracted, preImg and postImg are the L8 scene ID of pre-fire and post-fire L8 images, path and row the WRS-2 L8 frame identifiers, year is the reference year and area is the area of each polygon.

2.3.3 Computation of global BA accuracy metrics

This report summarizes the preliminary results obtained from the validation of FireCCI51 BA product for the year 2018. The approach detailed in section 2.3.2 was applied to the L8 2018 global archive for extracting reference fire perimeters over long validation units.

2.3.3.1 Computation of accuracy metrics

Reference fire perimeters and Fire_cci global BA products were intersected to estimate the following accuracy metrics: commission error ratio, omission error ratio, Dice Coefficient (DC) (Dice 1945), bias and relative bias (Table 3). The proportion of agreement or disagreement for all pixels of the TSA between the BA product (map) and the reference (Padilla et al. 2014; Padilla et al., 2017) (e_{ij}) used in the computation of the accuracy metrics is derived from the confusion matrix (Table 4).

Table 3. Accuracy metrics computed from the error matrix

Accuracy metric name	Formula
Commission error	$Ce = \frac{e_{12}}{e_{1+}}$
Omission Error	$Oe = \frac{e_{21}}{e_{+1}}$
Dice Coefficient	$DC = \frac{2e_{11}}{2e_{11} + e_{12} + e_{21}}$
Bias	$bias = e_{12} - e_{21}$
Relative Bias	$\boldsymbol{RelB = \frac{e_{21} - e_{12}}{e_{+1}}}$

Table 4. Sampled error matrix on a sampling unit. e_{ij} express the proportion of agreements (diagonal cells) or disagreements (off diagonal cells) between the BA product (map) class and the reference class. Proportions for all pixels is derived by summing up the proportion of agreement/disagreement for each pixel at the resolution of the BA products (lower spatial resolution).

Product classification	Reference classification		Row total
	Burned	Unburned	
Burned	e_{11}	e_{12}	e_{1+}
Unburned	e_{21}	e_{22}	e_{2+}
Col. total	e_{+1}	e_{+2}	

2.3.3.2 Preliminary results of accuracy metrics

At the time of writing of this document (October 2020) 92% of the 2018 TSAs were processed to estimate accuracy metrics for the FireCCI51 BA product. TSAs are distributed among the continents as follows: Europe (2), Africa (34), North America (7), Oceania (13), South America (8) and Asia (28). Table 5 summarizes Omission Error (OE), Commission Error (CE) and Dice Coefficient (DC) across biomes and Standard Error (SE) for each accuracy metric. Results are shown by biome and globally.

Table 5. Preliminary accuracy metrics of the 2018 FireCCI51 BA product computed by comparison with fire reference perimeters extracted from L8 long validation units. Quantitative figures refer to approximately 92% of the TSAs processed (N_{TOT}=100). Metric's value is reported together with Standard Error (SE) for each biome.

Biome	N/N_{tot}	OE		CE		DC	
		Value	**SE**	**Value**	**SE**	**Value**	**SE**
Boreal Forest	6/6	0.79	0.03	0.56	0.00	0.28	0.03
Mediterranean Forests	4/4	0.75	0.19	0.27	0.07	0.36	0.22
Savanna	36/42	0.40	0.05	0.14	0.03	0.70	0.04
Temperate Forest	8/8	0.14	0.06	0.15	0.03	0.85	0.03
Temperate Grasslands	10/11	0.53	0.02	0.35	0.04	0.54	0.02
Tropical Forest	15/16	0.92	0.06	0.46	0.05	0.12	0.09
Other	13/13	0.59	0.06	0.12	0.05	0.55	0.05
Global	**92/100**	**0.48**	**0.07**	**0.16**	**0.03**	**0.64**	**0.06**

These preliminary results are derived from all TSAs belonging to each biome (N in the first column) and for all biomes globally. **Overall**, estimated **omission and commission** errors for the 2018 **FireCCI51 BA product are 48% and 16%,** respectively. Biome level estimated errors are variable with highest omission errors for Tropical, Mediterranean and Boreal forests. Global estimated omission error is greater than commission as also shown by a relative bias of -38% (not shown in the table). The same occurs for per-biome error metrics with the exception of Temperate forests where the two errors are balanced (Relative Bias ~ 1.1%). These values are a consequence of the difference in spatial resolution of source reflectance data used for deriving the reference (Landsat 30 m) and FireCCI51 BA product (250 m).

The Dice coefficient provides a global measure of the error (by considering both omission and commission errors) with a global value of 0.64; best/greatest values (best agreement) are obtained for savanna and temperate Forest.

Hence, results show that, globally, burned area is underestimated as highlighted by OE and RelB values as also confirmed by Boschetti et al. (2019), who estimated accuracy metrics for one year of the Collection 6 NASA MCD64A1 500m global burned area product, and Chuvieco et al. (2018), who analysed multi-annual accuracy for global BA products FireCCI41, FireCCI50 and MCD64A1. Boschetti et al. (2019) estimated global commission and omission errors of 40.2% and 72.6%, respectively, with a very variable per-biome accuracy; highest errors were observed in Tropical and Temperate forests and Mediterranean biomes (OE >90%, CE >50%). Chuvieco et al. (2018) observed global commission and omission errors of 51.2% and 70.8%, respectively, for the FireCCI50 product, which is a previous version of the FireCCI51 BA products object of this report.

Indeed, FireCCI51 has been shown to provide improved burned area mapping accuracy with respect to its previous version (Moreno-Ruiz et al., 2020).

Several reasons could lay behind these results and among them. First, the minimum size of burned patches/areas detected by reference datasets derived from 30 m spatial resolution Landsat data is smaller than minimum size of burned areas derived from 250 m (FireCCI51) and 500 m (MCD64A1 Collection 6) global BA products. Furthermore, the length of the period of the validation units could also influence accuracy metrics. Finally, as highlighted by results presented here and by Boschetti et al. (2019), a significant variability of accuracy metrics can be observed for the difference biomes as a consequence of the fire/burns characteristics (e.g. type of fire, fire intensity, fragmentation of the fire patches).

Different sampling protocols of spatio-temporal validation units is another reason leading to large variability in accuracy metrics. Among all choice involved in the definition of a sampling protocol for identifying validation units in a random stratified sampling approach, the number of validation units per stratum is crucial since it is directly related to the effort needed for extracting reference perimeters and it can significantly influence estimated accuracy metrics.

Another issue to be considered when estimating accuracy of burned area products is the way reference and product burned area surfaces are compared. In Figure 14, burned area [m^2] derived from reference and FireCCI51 for single validation unit sampled in each biome is compared. General underestimation of the FireCCI51 BA products is confirmed by the point laying below the 1:1 line as expected by coarser resolution products and consistently with published results (Boschetti et al., 2019).

The specific case of the Boreal Forest biome deserved further analysis to investigate factors determining the estimated error metrics (Table 5). Out of the 6 validation units sampled for this biome (Asia=2 high fire activity+ 2 low fire activity, North America=2 low fire activity), four were not affected by fires during 2018 as observed in both reference and FireCCI51 datasets. For remaining validation units, very small burned surface was observed in the reference dataset and over the period covered by the validation long units to total about 32 km^2; this burned surface was only partially detected in the FireCCI51 BA product due to the small size of burned polygons. Yet when agreement and disagreement between reference and product burned surfaces are "converted" into ratio error metrics (Table 3) large percentages are obtained despite the small surfaces involved.

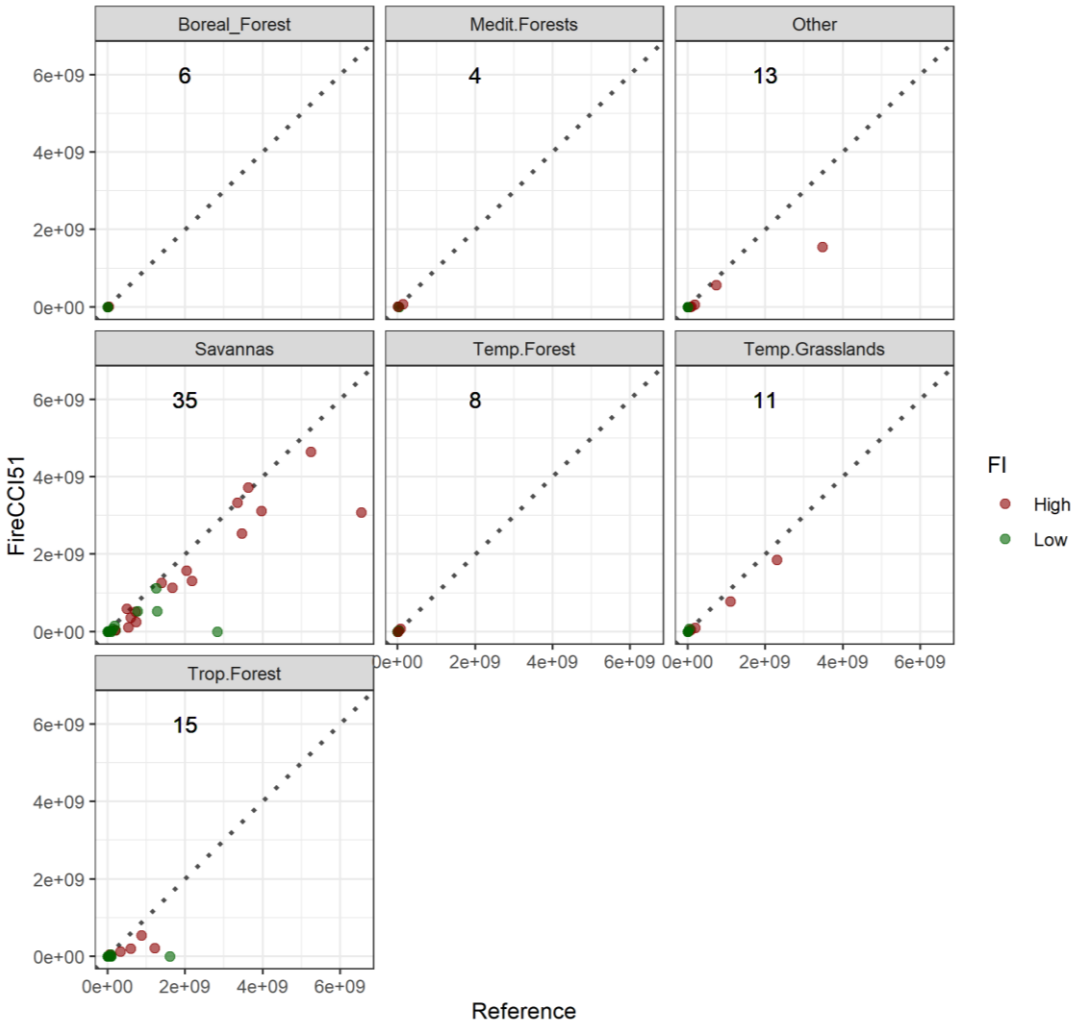

Figure 14: Scatter plots of reference (x-axis) and FireCCI51 (y-axis) burned area [m^2] for each validation unit and biome. Each point is filled with red and green to represent validation units in the high and low fire activity straum for each biome, dotted line shows full agreem (1:1) and the number shows the total units sampled per biome.

In the figures below, comparison examples between fire reference perimeters over two TSAs in savanna (Africa) are shown. In the first case (Figure 15) several small burned areas are not identified by the FireCCI51 BA product (blue regions: BA Oe) due to the difference of spatial resolution of the source EO data used for BA product (MODIS 250 m) and reference perimeters (Landsat 30 m). In the zoomed area, omission errors are highlighted by blue areas; in this example, omission errors (OE=0.81) lead to a Dice Coefficient of 0.29. In the second case (Figure 16), a satisfactory agreement between reference and FireCCI51 BA product is achieved (shown by the large portion of green area) leading to a Dice Coefficient equal to 0.85. In this second example, the commission error rate is very low (CE=0.08).

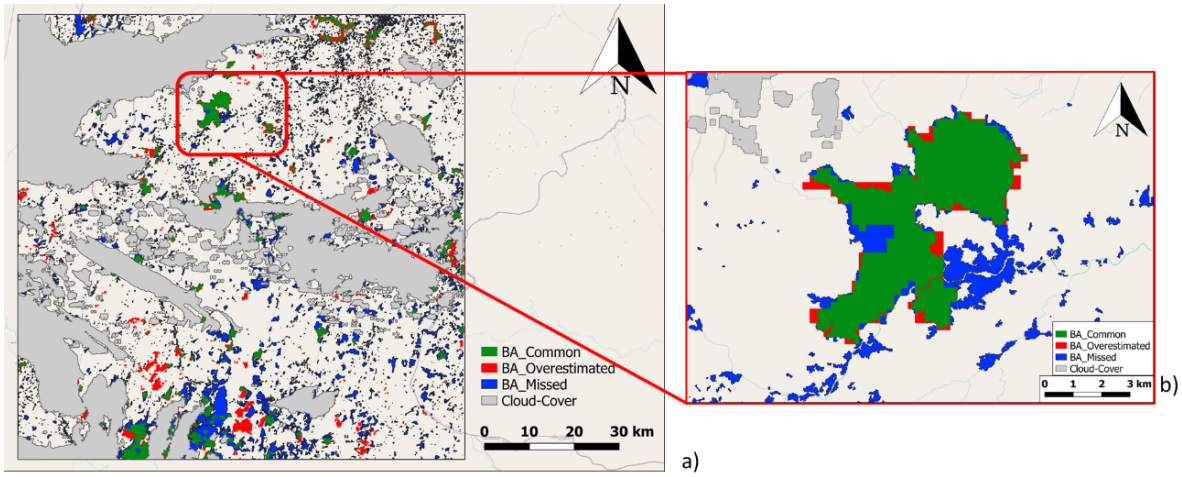

Figure 15: Comparison example of 2018 reference fire perimeters and FireCCI51 burned area maps over L8 TSA 178/054 (L8 path/row) (Savanna, Africa). Agreement areas are green while commission and omission errors are red and blue, respectively. In this case accuracy metrics are: omission error OE=0.81, commission error CE=0.43, dice coefficient DC=0.29.

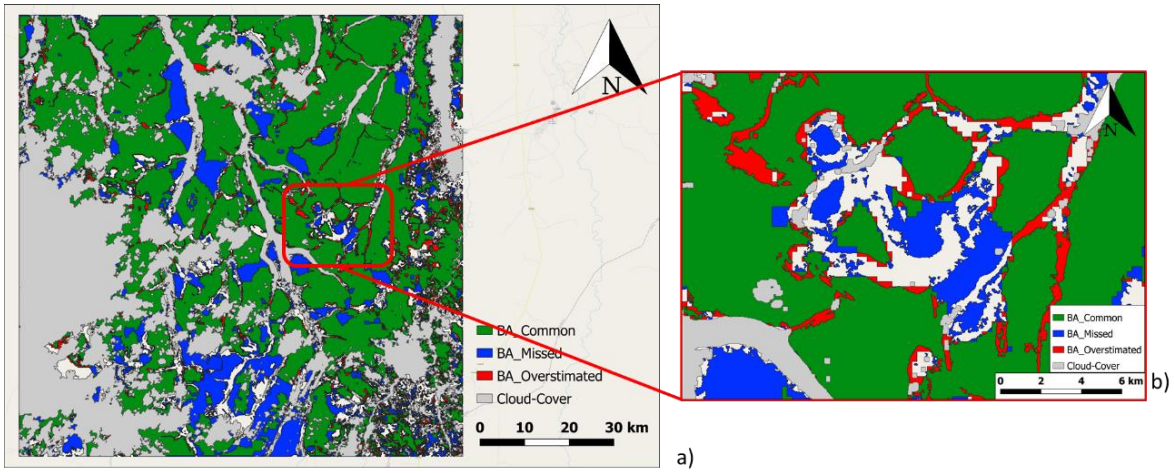

Figure 16: Comparison example of 2018 reference fire perimeters and FireCCI51 burned area maps over L8 TSA 178/066 (L8 path/row) (Savanna, Africa). Agreement areas are green while commission and omission errors are red and blue, respectively. In this case accuracy metrics are: omission error OE=0.20, commission error CE=0.08, dice coefficient DC=0.85.

Figure 17 shows Omission and Commission errors, the Dice coefficient and the Relative Bias for each biome. With respect to results shown in Table 5, these figures are extracted globally by summarizing comparison between reference and FireCCI51 carried out for each TSAs. Global values highlight some differences with respect to average values in Table 5 for the boreal forest biome, in particular, that it shows an omission error comparable to the tropical forest biome.

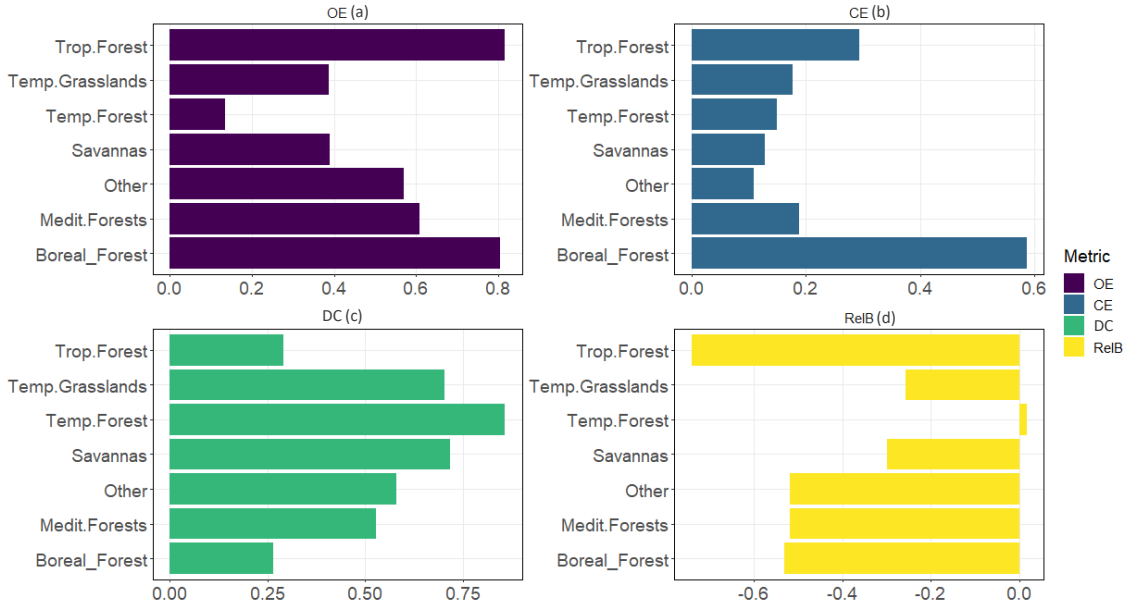

Figure 17: a) Omission error (OE), b) Commission error (CE), c) Dice Coefficient (DC) and d) Relative Bias (RelB) for each biome.

In brief, the results presented for the validation of global FireCCI BA product for the year 2018 highlighted some issues that will be further addressed and analysed in the next months of project activity:

- Influence of sampling approach (identification of the sampling validation units in time and space and their cardinality across strata) on error metrics;
- Criteria and products exploited for stratification into high and low fire activity;
- Estimated accuracy of validation units with low burned surface and/or no fire activity;
- Comparison of agreement and disagreement of burned surfaces through confusion matrix and error metrics as well as regression analysis.

2.4 Validation of regional/continental BA product

In this phase of the Fire_cci project, the **Sentinel-2 Small Fire Database (SFD)** (FireCCISFD11) (Roteta et al., 2019) will be produced for the year **2019** over the Sub-Saharan African continent; the product is derived by processing S2 images acquired during a single year at continental scale (all Africa below 25° N latitude). In order to validate the BA product, a specific sampling scheme was designed for locating spatio-temporal validation units. The scheme proposed in the following sections builds on the experience inherited from the L8 sampling approach implemented at global scale (2.3.1); the L8 protocol for the selection of the validation units was adapted to consider the peculiarities of S2 acquisitions and the ESA tile format. The same random stratified sampling approach was applied and strata were identified from the same sources of information: biomes and fire intensity.

Since the size of the validation units was set to 100 km by 100 km, S2 tiles were directly used for spatial sampling. In order to identify, within the S2 archive, the population of tiles suitable for sampling and covering Sub-Saharan Africa, two additional selection criteria were defined to cope with S2 tiles encompassing different orbits and overlapping at the border of UTM zones (2.4.1).

2.4.1 S2 sampling scheme and implementation

2.4.1.1 S2 sampling stratification

Validation units were defined from spatio-temporal partition of S2 2019 archive over sub-Saharan Africa (latitude range 25°N- 35°S). Since each unit covers an area of 100 km x 100 km and S2 tiles are 10,000 km^2 ortho-images in UTM/WGS84 projection, S2 tiling grid was directly used for spatial partition. However, in order to provide robust statistical sampling and avoid overlapping between units, two additional criteria were applied to select suitable S2 tiles.

First, S2 tiles whose footprint crosses different orbits, as shown by yellow polygons in Figure 18a, were discarded and only tiles fully covered by a single orbit were retained. An example of the 100x100 km S2 tile area fully and partially covered by a single orbit is given in Figure 19a and Figure 19b, respectively. For the two tiles shown in the example, only the second one (Figure 19b) is retained since data are acquired on a single date.

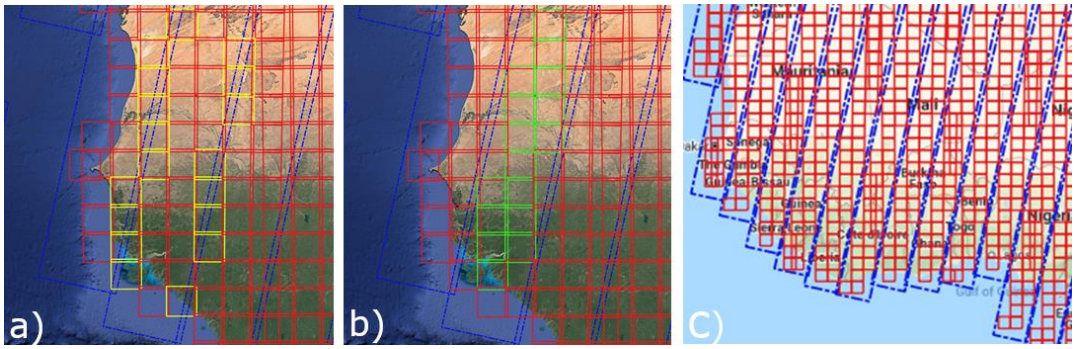

Figure 18: a) example S2 tiles not suitable (yellow) as TSAs for sampling since they cover different orbits; b) example S2 tiles suitable (green) as TSAs for sampling since they cover the same orbit; c) all S2 tiles suitable for sampling in the example area in Eastern Sub-Saharan Africa.

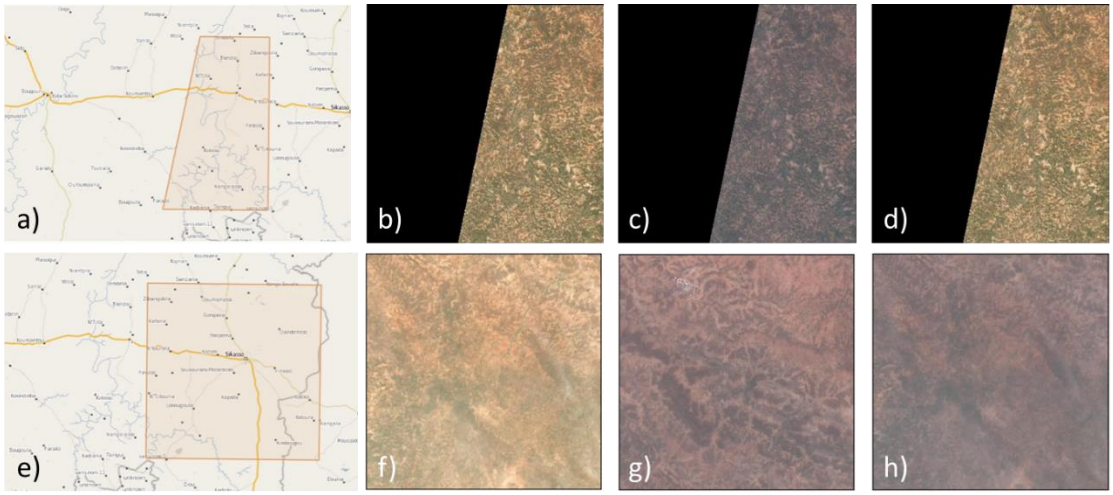

Figure 19: Examples of S2 tile images, as available from Copernicus Open Access Hub (https://scihub.copernicus.eu), for data acquired over Relative Orbit 008 (R008). Top row shows S2 images over tile T29PQN (partially covered by the orbit R008) acquired at different dates in 2020; bottom row shows tile T29PRN (fully covered by R008).

Second, nearby the boundaries between adjacent zones of UTM coordinate projection system, S2 data are provided on partially-overlapping tiles archived with different

Universal Transverse Mercator (UTM) projection (yellow polygons in Figure 20a). In these conditions, keeping both overlapping tiles would increase sampling probability of the common area. In order to address this issue, among the pairs of S2 tiles overlapping due to different UTM zones, only one was randomly selected and retained (Figure 20b).

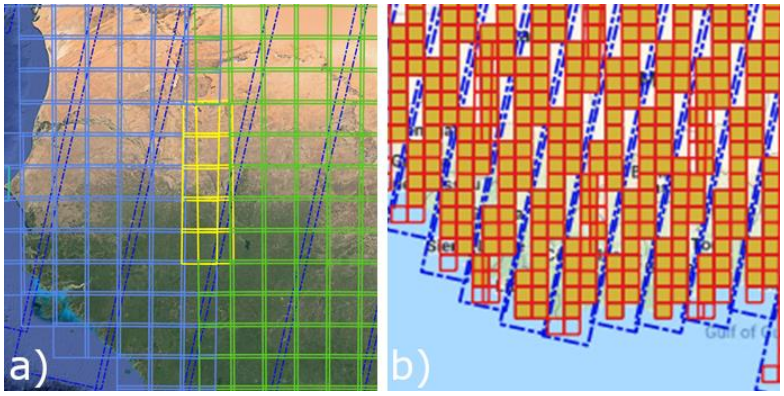

Figure 20: a) example S2 tiles not suitable (yellow) as TSAs for sampling since they overlap due to overlapping UTM zones; b) example S2 tiles suitable (orange) as TSAs for sampling after random selection.

Once the two previous filtering conditions are applied to the S2 tiling grid system, the population of tiles suitable as validation units is composed of the subset of tiles shown in Figure 21a. For each of these tiles, i) the total annual burned area from the 2019 FireCCI51 BA product (Figure 21b) and ii) the major Olson biomes (Figure 21c) were computed. As in the case of the Global BA validation (section 2.3.1.1), the intersection of these two layers provides strata for implementing stratified random sampling (Figure 23).

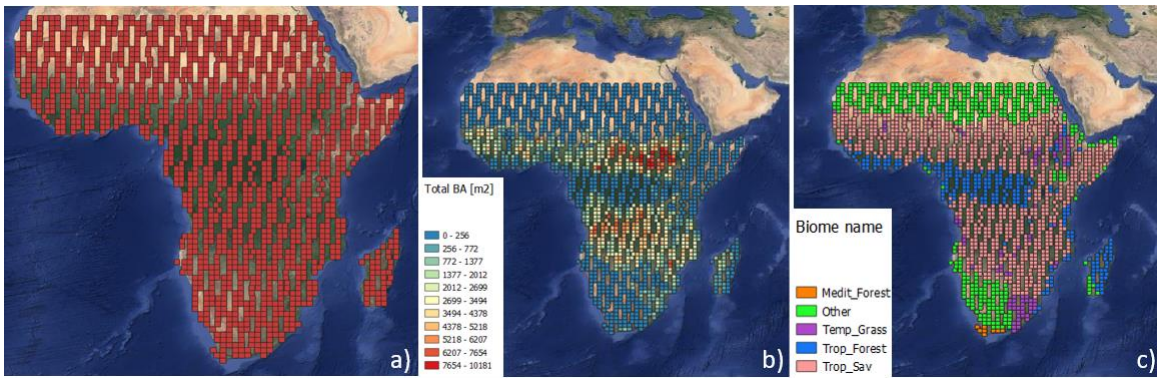

Figure 21: a) S2 tiles available for sampling after applying criteria outlined previously in this section; b) total burned area for each S2 [m^2]; c) Major Olson biome for each S2 tile.

In particular, the 2019 FireCCI51 BA product was exploited to divide each Olson biome into sub-strata of high and low fire intensity by applying a threshold derived as in section 2.3.1.1.

In order to assign the high/low fire intensity class, the total annual burned area (TotBA, m^2) was computed in each S2 tile and these values were then sorted in increasing order; the cumulated sum was computed and normalized with respect to the biome's maximum value of total annual BA. The TotBA value corresponding to the 20^{th} percentile of the normalized cumulated sum (Padilla et al. 2017, Boschetti et al., 2016) provides the threshold for assigning each S2 to either the ***high*** (total annual BA > threshold) or ***low*** (total annual BA <= threshold) fire intensity classes. In Figure 22, threshold values for

each biome and the year 2019 are reported in blue colour; values are also summarized in Table 6.

Table 6. Threshold values identified for stratification of each biome into high/low fire intensity strata. The number of high and low fire intensity TSAs for each biome and the year 2019 is also reported.

Biomes	Threshold [km^2]
Boreal Forest	-
Mediterranean Forests	364
Savannas	2367
Temperate Forest	-
Temperate Grasslands	1646
Tropical Forest	620
Other	103

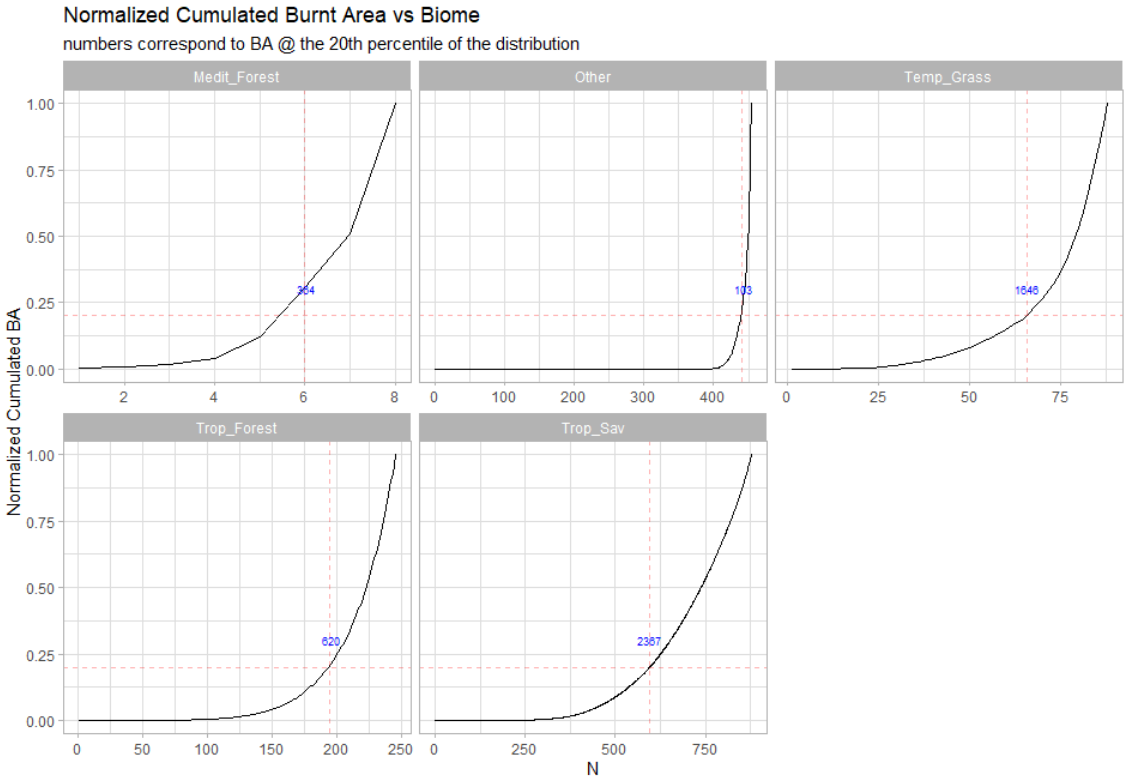

Figure 22: S2 tiles for each biome plotted by increasing value of normalized total annual burned area; on the x-axis the cumulated number of S2 tiles (N). The red dashed horizontal line shows the 20th percentile and the corresponding value of total annual burned area used for assigning each tile to high/low intensity fire classes is highlighted in blue.

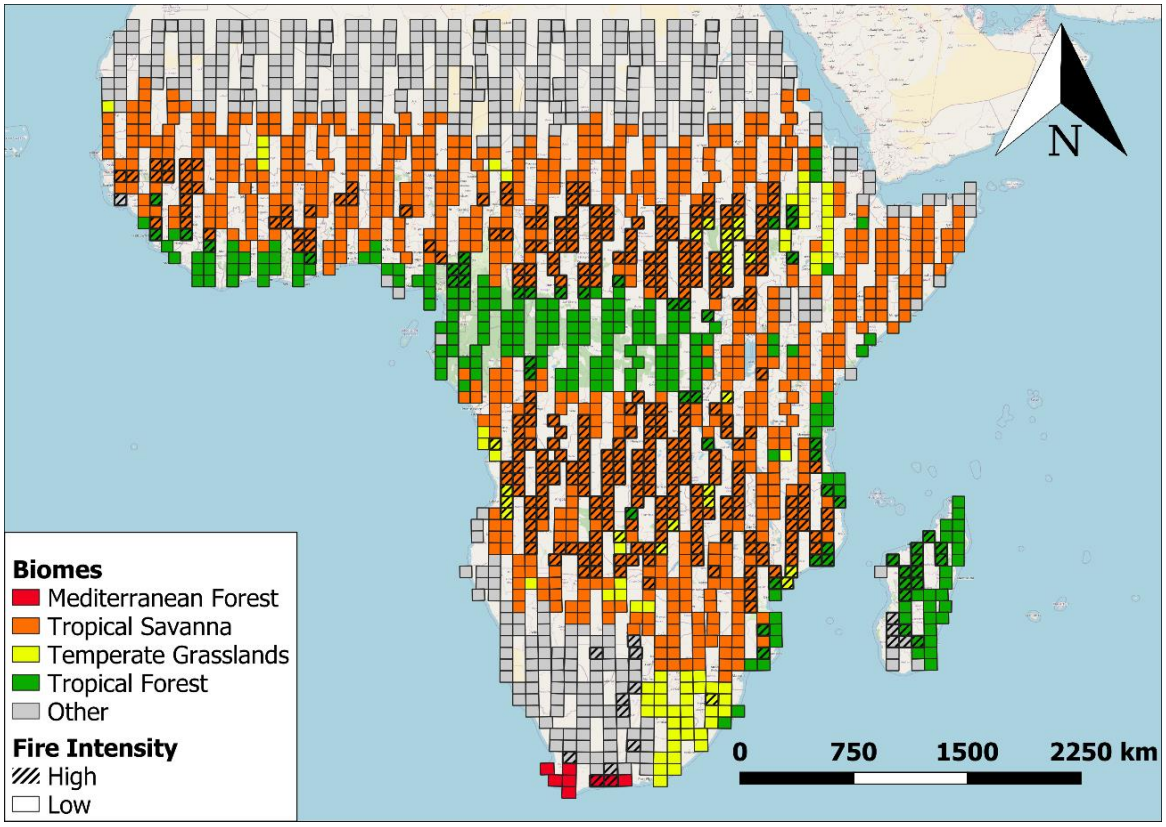

Figure 23: S2 tiles suitable for sampling for each stratum (intesection between biome and high/low fire intensity).

2.4.1.2 Analysis of S2 data availability 2019

Preliminary analysis of data availability over the population of S2 tiles available for sampling was carried out for the year 2019 (as done for global L8, see section 2.3.1.2). The S2 archive was inspected to identify, for each tile, the S2 temporal series **with maximum time step (Δt_{max}) of 16 and/or 32 days between pairs of consecutive clear-sky images.** In this context, S2 images are considered to be "clear-sky" if their cloud coverage percentage is lower than 30%. Information on cloud coverage percentage is extracted from the S2 metadata and, specifically, the sum of *"High probability clouds percentage"* and *"Medium probability clouds percentage"* was assumed as total cloud cover.

Figure 24 shows the length [L, days] of the validation long units over S2 tiles suitable for sampling computed by considering Δt_{max}=16 days (panel a) and Δt_{max}=32 days (panel b). The length of the unit ranges between minimum values in the tropical regions (below 30 days) and maximum values for the northern and southernmost areas and desertic regions (greater than 300 days).

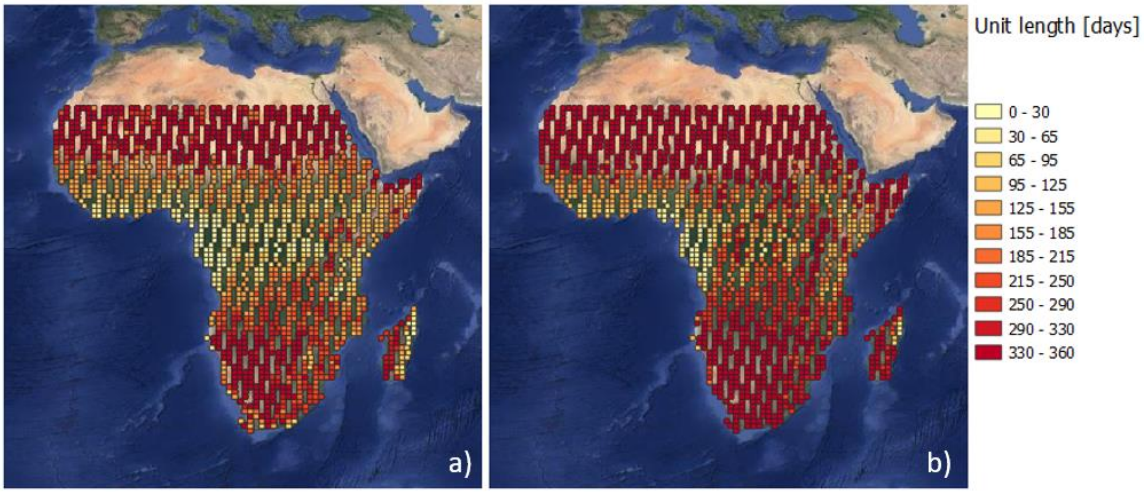

Figure 24: Length [days] of the long validation units over S2 tiles available for sampling, computed considering maximum time step between consecutive scenes (Δt_{max}) of 16 (panel a) and 32 days (panel b).

Results shown in Figure 24a are also shown as histogram plot in Figure 25 where the total number of tiles available for sampling is plotted against series length L [days]. If biome and fire intensity stratification is considered, S2 tiles available for sampling are distributed across biomes as a function of the minimum series length L [days] as shown in Figure 26 and Figure 27; series length values are shown on top of each panel.

As observed for global L8 validation units, the number of units available for sampling is greater in the low intensity fire stratum and decreases with the increase of minimum length L.

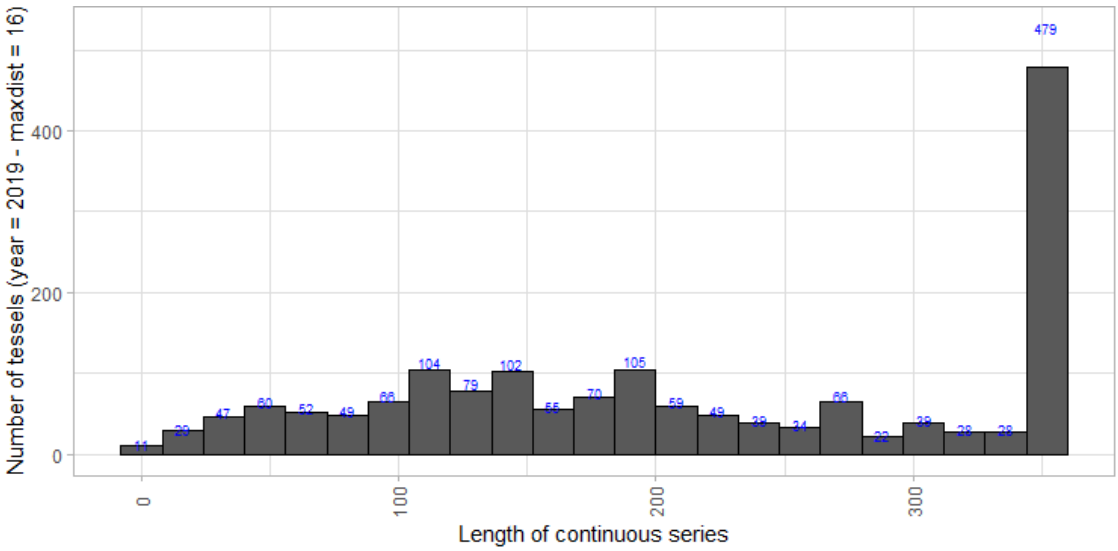

Figure 25: The total number of S2 tiles available for sampling over Africa as a function of the length L of the long unit [days] and computed for consecutive scenes with maximum time step of 16 days.

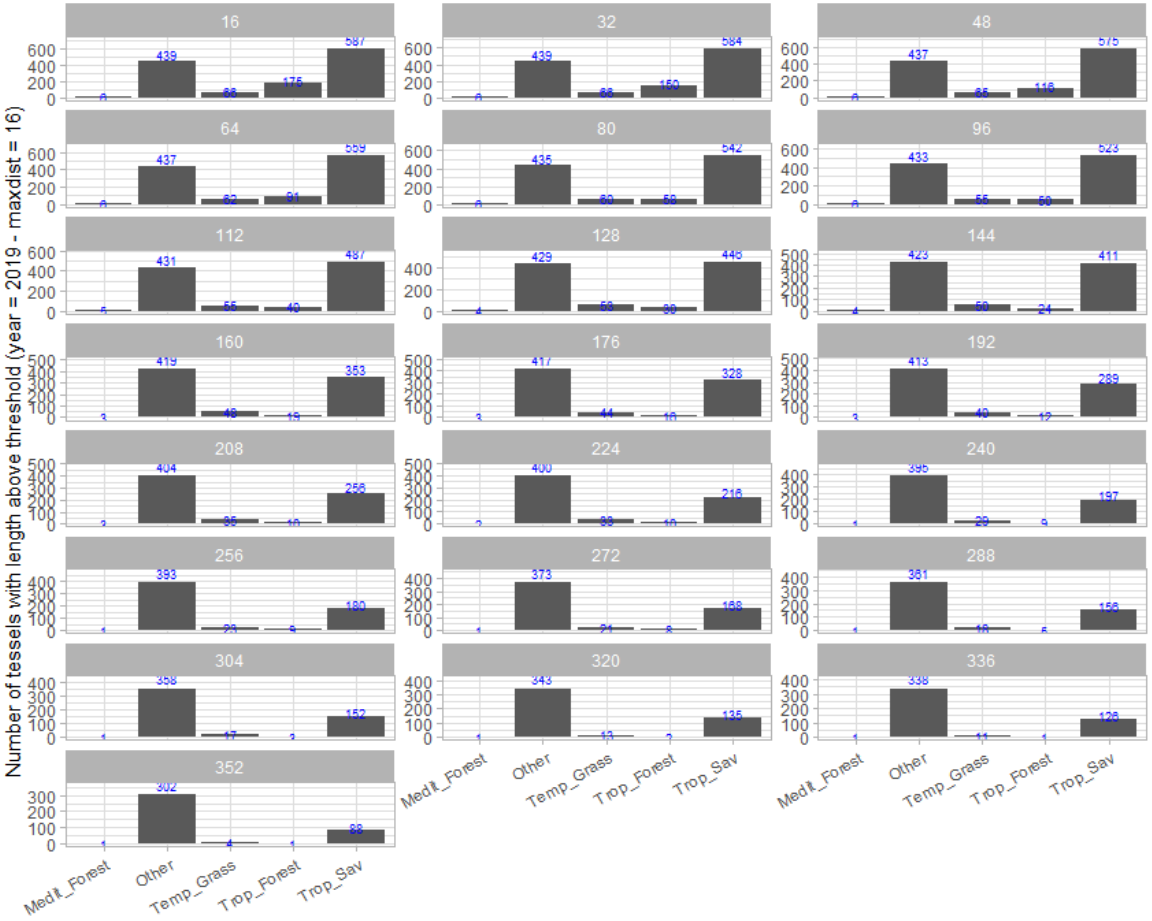

Figure 26: Number of suitable S2 tiles for each biome in the Low Fire Intensity class as a function of the minimum length of the of the unit (L) (shown on top of each panel as number of days). Maximum time step between S2 consecutive pairs is set to 16 days and blue values show the number of available S2 tiles when length L is greater than the value shown on the top bar.

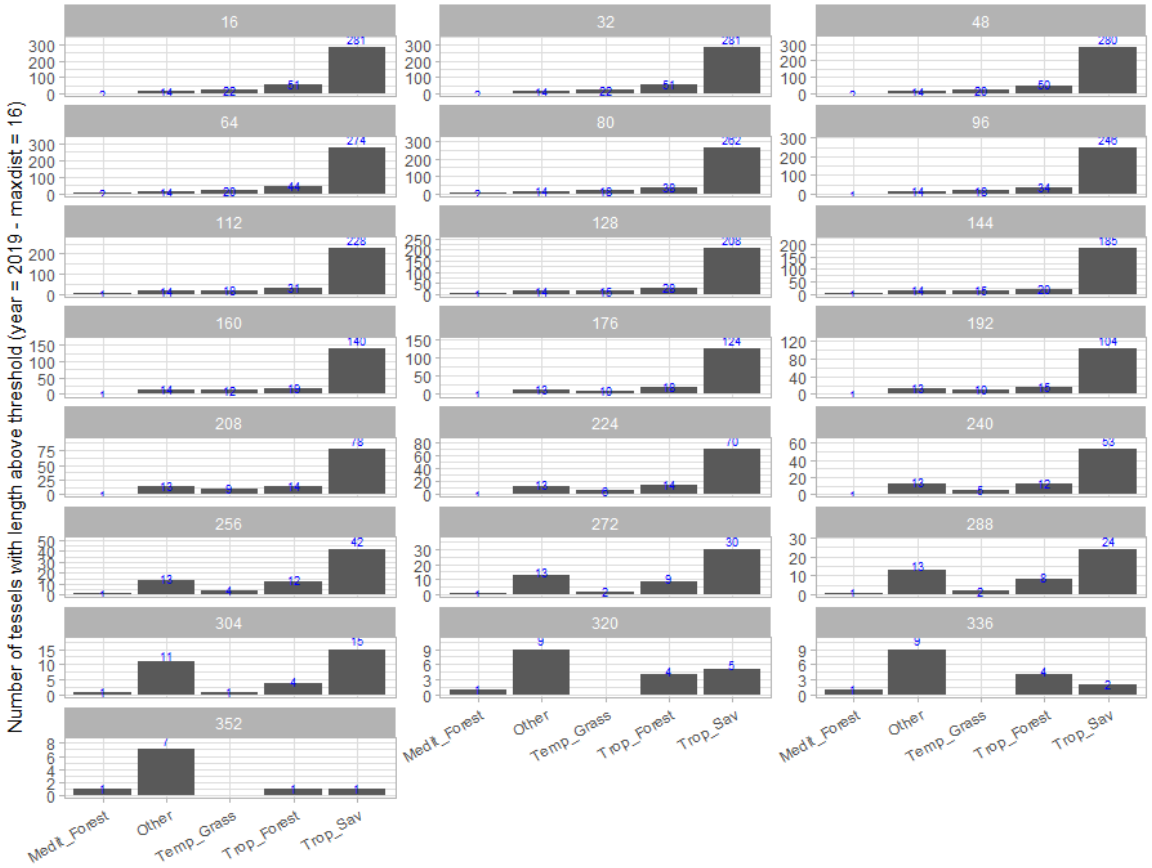

Figure 27: Number of suitable S2 tiles for each biome in the High Fire Intensity class as a function of the minimum length of the of the unit (L) (shown on top of each panel as number of days). Maximum time step between S2 consecutive pairs is set to 16 days and blue values show the number of available S2 tiles when length L is greater than the value shown on the top bar.

A minimum length of the validation unit was set to 100 days, since this value assures a suffcient representation of the smallest strata. Hence, **hereafter sampling is carried out from the population of suitable S2 tiles with Δt_{max}=16 days and L_{min}=100 days.**

2.4.1.3 S2 Sampling cardinality

A total of **50 validation** units/tiles were extracted from the suitable population identified in 2.4.1.1 (Δt_{max}=16 days and L_{min}=100 days) and they were distributed among strata based on Eq. 2.

$$n_h \propto N_h \sqrt{\overline{BA}_h} \qquad \text{Eq. 2}$$

where n_h is the number of S2 tiles to be sampled for stratum h, $\overline{BA}_h$ is the average total annual (2019) burned area for stratum h and N_h is the total amount of S2 tiles available for sampling for stratum h. For smaller strata, a minimum of n_h= 2 is assigned. Results obtained with this procedure are summarized in Table 7: the reported number of S2 tiles for each stratum was randomly sampled from the S2 tiles suitable for sampling. The location of the sampled tiles is shown in Figure 28.

Table 7. For each stratum, the number of S2 tiles available/suitable for sampling (N_h) and the number of S2 tiles to be sampled (n_h) according to Eq. 2 for the year 2019 over Africa. N_h is computed from the S2 archive by setting Δt_{max}=16 days and L_{min}=100 days.

Biomes	N_{HIGH}	N_{LOW}	FI_{high}	FI_{low}	Total
Boreal Forest	-	-	-	-	-
Mediterranean Forests	2	6	2	2	4
Savannas	281	596	20	14	34
Temperate Forest	-	-	-	-	-
Temperate Grasslands	22	66	2	2	4
Tropical Forest	51	194	2	2	4
Other	14	440	2	2	4
Total	**370**	**1302**	**28**	**22**	**50**

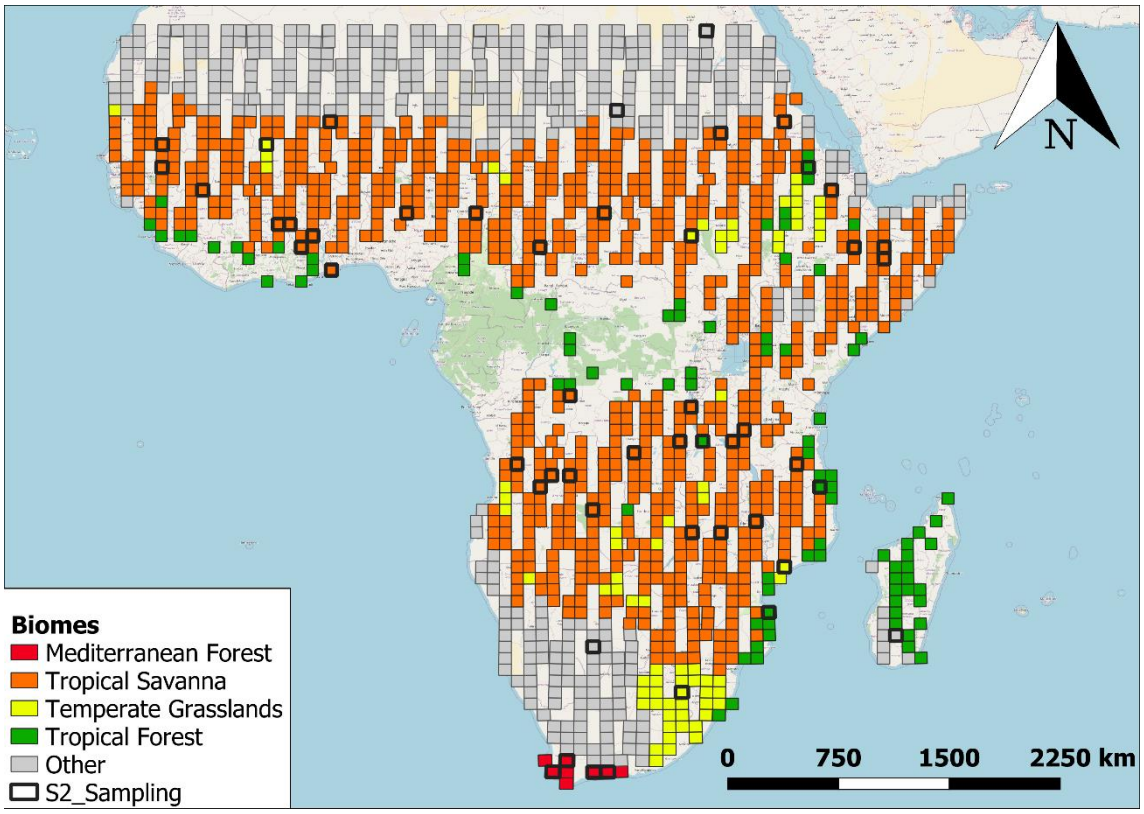

Figure 28: Spatial distribution of the 50 S2 tiles sampled randomly over Africa for each stratum (biome/fire insentity) highlighted in black and overlaid on the S2 tiles suitable for sampling as extracted from the S2 archive by setting Δtmax=16 days and Lmin=100 days..

2.4.2 Extraction of S2 fire reference perimeters

Fire perimeters for S2 validation units were extracted for short units (consecutive S2 images) to map areas burned between the two dates (t1, t2); processing steps are the same as L8 and the flowchart is shown in Figure 2. All short units over the same area are combined to derive fire perimeters over the S2 long unit with a script coded in Arcpy.

S2 short unit classification was implemented in GEE that applies a RF algorithm to identify burned polygons; the script is coded to perimeter existing burned areas between two consecutive images. Details on script input/output are provided in 2.3.2. The output layers consist of:

- Burned areas in vector KML format;
- The validation region of 100 km x 100 km obtained by a buffering of the centroid of the S2 frames;
- Cloud Mask in vector format;
- Training polygons as vector shapefiles;

The classification of the S2 short units is then converted to shapefile format and processed to extract fire reference perimeters, clouds and burn date.

At the time of writing of the present report, the protocol for sampling S2 validation units has been defined and implemented to extract the suitable S2 tiles. Fire reference perimeters will be extracted and delivered by the end of September 2020.

However, an example S2 tile is given in Figure 29 and Figure 30. Figure 29 shows a time series of cloud-free S2 images with maximum time step between consecutive dates of 16 days for S2 tile 35MLN (Democratic Republic of Congo, DRC). The corresponding BA product covering the entire validation period is shown in Figure 30.

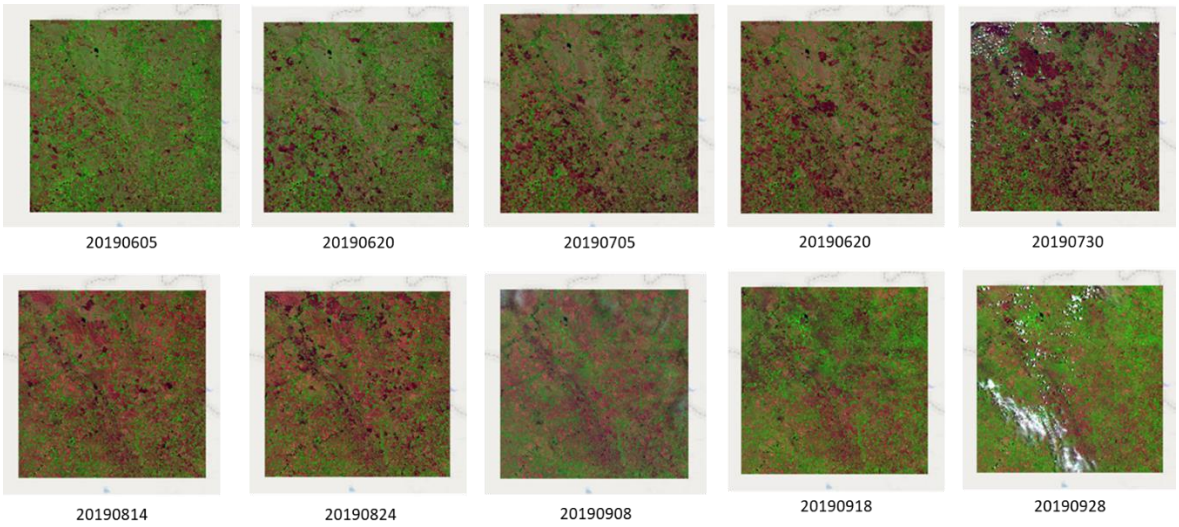

Figure 29: Time series of cloud-free S2 images for S2 tile 35 MLN (DRC) and displayed as RGB false colour composites (SWIR-NIR-Red).

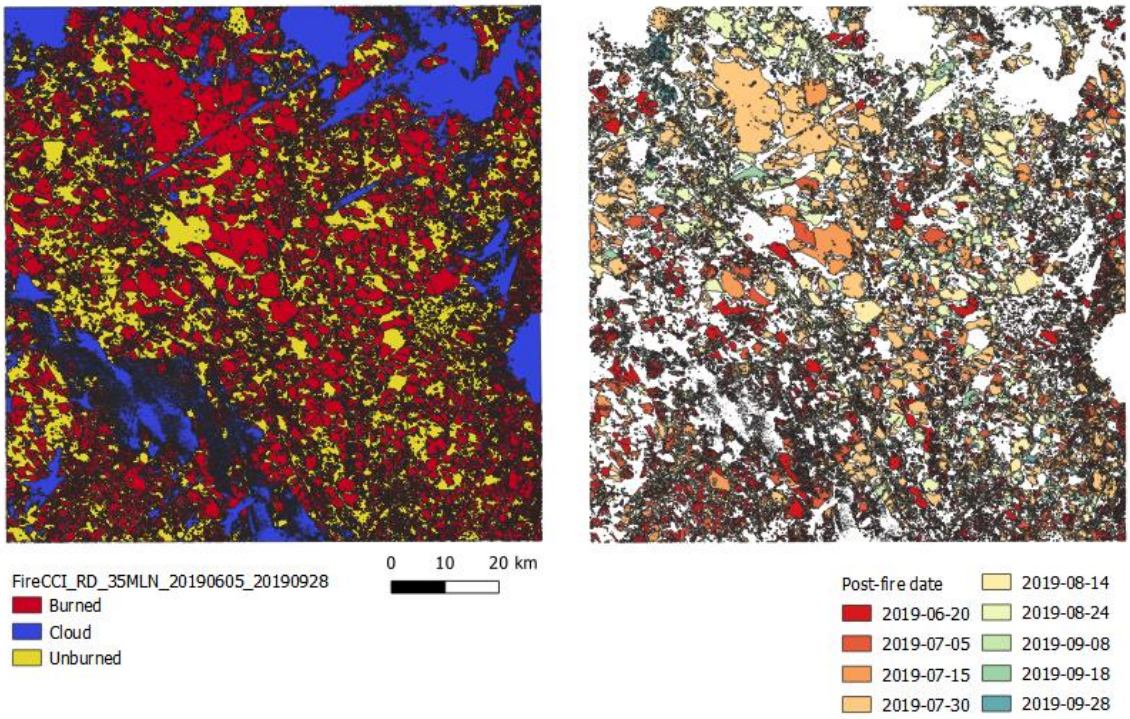

Figure 30: BA reference perimeters for S2 tile 35 MLN (DRC, Africa) as obtained from time series of cloud-free S2 images (Figure 29) and a RF algorithm: a) synthetic final BA map showing over the period June 05 to September 28, 2019, burned polygons (red), clouds (blue) and unburned polygons (yellow); b) BA polygons displayed with post-fire date attribute.

2.5 Validation of BA product over S1&S2 test sites

In this section, the source data and methodology for extracting fire reference perimeters over validation sites of the SAR-O algorithm are described.

2.5.1 Planetscope source data

Over the three study sites for testing the SAR-O algorithm that exploits integration of S1 and S2 for high resolution burn mapping (Figure 31), no stratified sampling design is applicable (validation at stage 1). Hence, within each test area, validation units were selected to cover different fire, land cover and cloud cover conditions. The availability of High resolution (HR) Planetscope data (https://www.planet.com/) was inspected for spot/local evaluation of the Fire_cci BA products and Planetscope scenes were downloaded over a set of validation units within the three sites shown in Figure 31. Cloud free images were selected to cover a period of about two/three months.

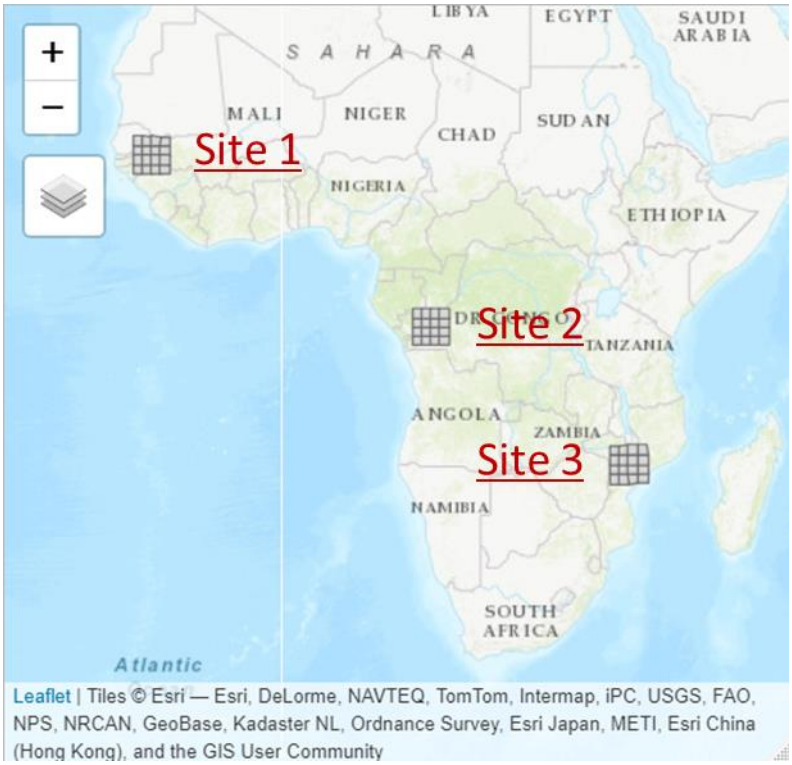

Figure 31: Location of the sites of interest for SAR-O algorithm deployment: Site 1 Northern Africa, Site 2 Central Africa and Site 3 Southern Africa.

PlanetScope is a constellation composed by more than 120 optical satellites (also named Doves) operated by Planet from 2016. Each Dove satellite is a CubeSat 3U form factor (10 cm by 10 cm by 30 cm) (https://earth.esa.int/web/guest/missions/3rd-party-missions/current-missions/planetscope, accessed July 2020). The sensor mounted on this platform is characterized by four acquisition bands: three in the visible wavelengths (b1: 455-515 nm; b2: 500-590 nm; b3: 590-670 nm) and one in the NIR wavelengths (b4: 780-860 nm). Planetscope has a swath of about 25 Km. The spatial resolution of PlanetScope images is 3 m for all bands. Imagery is captured as a continuous strip of single frame images known as "scenes". Table 8 summarizes PlanetScope mission and sensor characteristics (Lemajic et al., 2018).

Table 8. PlanetScope Constellation and Sensor Specifications (Source: Lemajic et al., 2018).

MISSION CHARACTERISTICS	SUN SYNCHRONOUS ORBIT
Orbit altitude (reference)	475 Km (-98° inclination)
Max/min latitude coverage	± 81.5° (depending on season)
Equator crossing time	9:30 – 11:30 am (local solar time)
Sensor type	Three-band frame imager or four-band frame imager with a split-frame NIR filter
Spectral bands	Blue 455-515 nm Green 500-590 nm Red 590-670 nm NIR 780-860 nm

MISSION CHARACTERISTICS	SUN SYNCHRONOUS ORBIT
Ground sampling distance (nadir)	3.7 m (at reference altitude 475 Km)
Swath width	24.6 Km x 16.4 Km (at reference altitude)
Maximum image strip per orbit	20.000 Km2
Revisit time	Daily at Nadir (early 2017)
Image capture capacity	150 million Km2/day (early 2017)
Camera dynamic range	12-bit

Table 9 summarizes Planetscope images downloaded at the time of writing of this document (July 2020) over sites 1 to 3 (Figure 31). For each validation site, smaller regions were identified that were covered by approximately ten Planetscope scenes. The multi-temporal dataset was selected from the most cloud free dates. Selection and downloading of Planetscope images are still on progress; site 2 (central Africa) is characterized by the least images available due to persistent cloud cover.

Table 9. Planetscope images downloaded at the time of writing of this report: validation site, sub-site, location name and dates.

Site		Location	Dates	Number of scenes	Projection
Site 1	A	Tambacounda (Senegal)	14/01/2019	10	UTM 28 N
			21/01/2019	10	
			28/01/2019	11	
			17/02/2019	12	
			25/02/2019	13	
			28/02/2019	15	
			09/03/2019	14	
			12/03/2019	14	
	B	Niokolo_Koba (Senegal)	17/01/2019	8	UTM 28 N
			30/01/2019	8	
			06/03/2019	8	
			20/03/2019	9	
Site 2	A	Yola (Democratic Republic of Congo)	05/06/2019	13	UTM 33 S
	B	Kinshasa (DRC)	08/06/2019	12	UTM 33 S
Site 3	A	Capenga (Mozambique)	30/07/2019	9	UTM 36 N
			05/09/2019	4	
			11/09/2019	8	
			29/09/2019	9	
			26/10/2019	8	

Figure 32 shows along track mosaics of Planetscope images. In particular, panel a shows the two sites A (Tambacounda) and B (Niokolo_Koba) in Senegal while panel b shows the site A (Capenga) in Mozambique. Figure 33 presents an example of the mosaic images derived from single Planetscope scenes over Site 1B; images are shown as RGB false

colour composites (NIR-Red-Green). Progress of burned surfaces can be observed as the fire season proceeds from January to March.

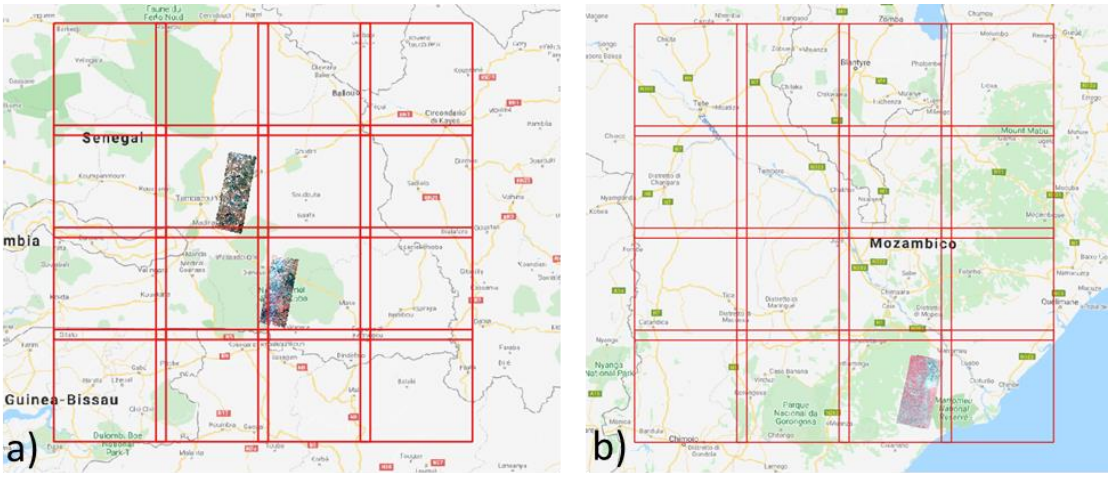

Figure 32: The location of sites 1A, 1B and 3A within the validation sites in Northern Africa (a) and southern Africa(c).

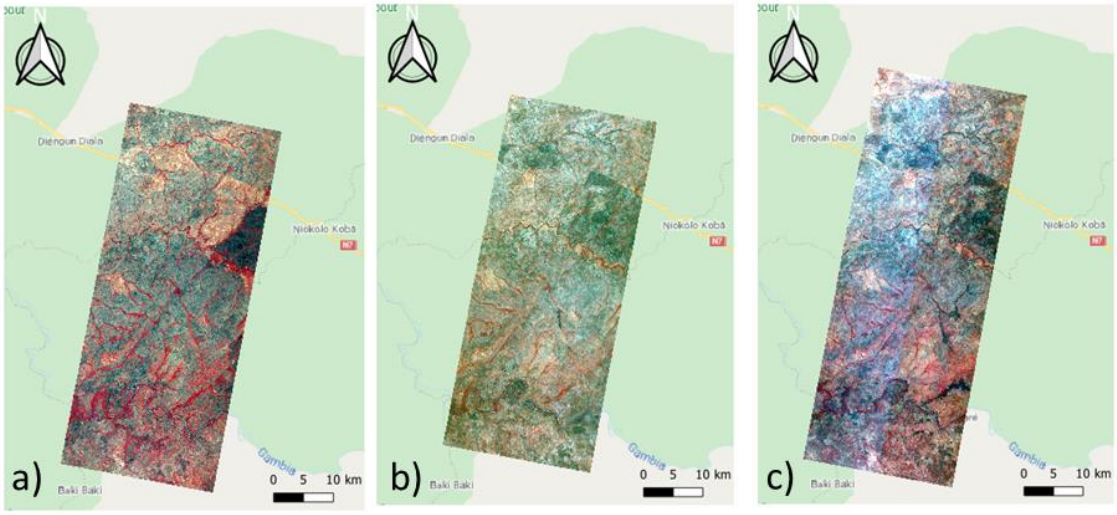

Figure 33: Example Planetscope image mosaics displayed as false colour composites (RGB; NIR, Red, Green) over site 1 B for the following dates: 30/01/2019 (a), 06/03/2019 (b) and 20/03/2019 (c).

2.5.2 Extraction of Planetscope fire reference perimeters

Preliminary tests were carried out for defining the best approach for the extraction of fire reference perimeters from Planetscope images. Results shown in Figure 34 and Figure 35 were derived from processing Planetscope image mosaics acquired over Site 3A (southern Africa, Capenga, Mozambique). Two sets of scenes were selected to identify the areas that burned between two dates (pre- and post-fire): 29/09/2019 (9 scenes) and 26/10/2019 (8 scenes) with a supervised Random Forest (RF) classification algorithm. Single scenes were processed to derive mosaic image for each date (using "merge" raster function in QGIS); the output of this step are two geo-tiff files for pre-fire and post-fire dates. Afterwards, the NDVI was computed for each date from the NIR and Red bands of the Planetscope images. This step was performed using the "raster calculator" command of QGIS.

Then temporal differences between pre- and post-fire dates ($\Delta_{post-pre}$) of all Planescope bands and NDVI were calculated as shown in Figure 34. The stack layer of spectral reflectance and NDVI bands for post-fire date and temporal difference $\Delta_{post-pre}$ was used as input to the classification algorithm.

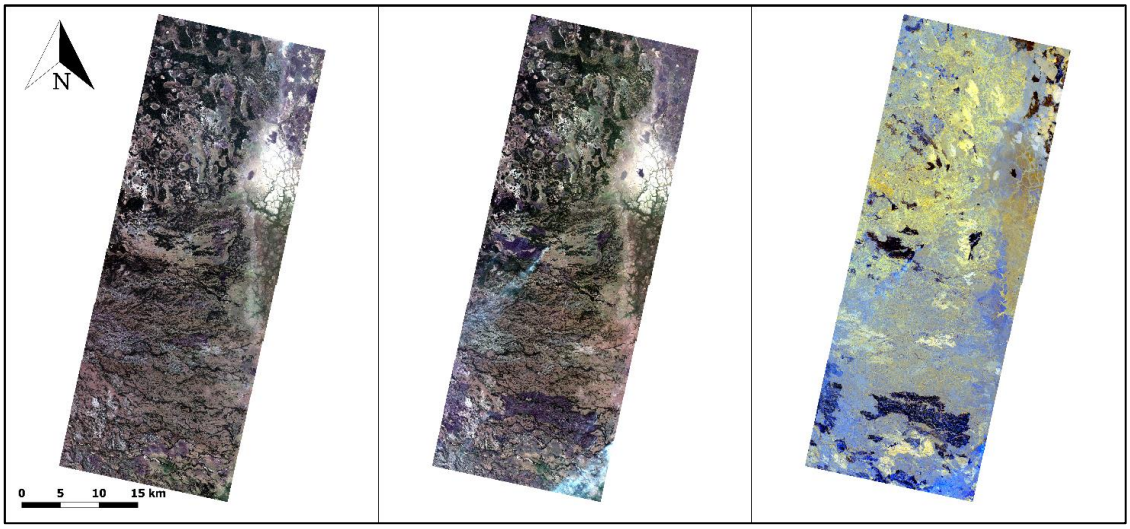

Figure 34: On the left: true colour Planetscope image acquired on 29/09/2019. In the middle: true colour Planetscope image acquired on 26/10/2019. On the right: false colour composite of temporal difference image $\Delta_{post-pre}$ (NDVI, NIR, Red).

The classification into burned/unburned was performed with a RF algorithm by manually defining training areas by photointerpretation of temporal difference reflectance and NDVI. The RF algorithm is implemented in the QGIS plugin "dzetsaka classification tool" (https://github.com/nkarasiak/dzetsaka, last access July 2020). The algorithm was applied iteratively by adjusting the training areas over burned and unburned areas to derive the best classification. The output raster is characterized by a spatial resolution of 3 meters (the same as Planetscope input images) and represents the area burned between 29/09 and 26/10, 2019. An example of the input image and output classification (burned/unburned) is shown in Figure 35.

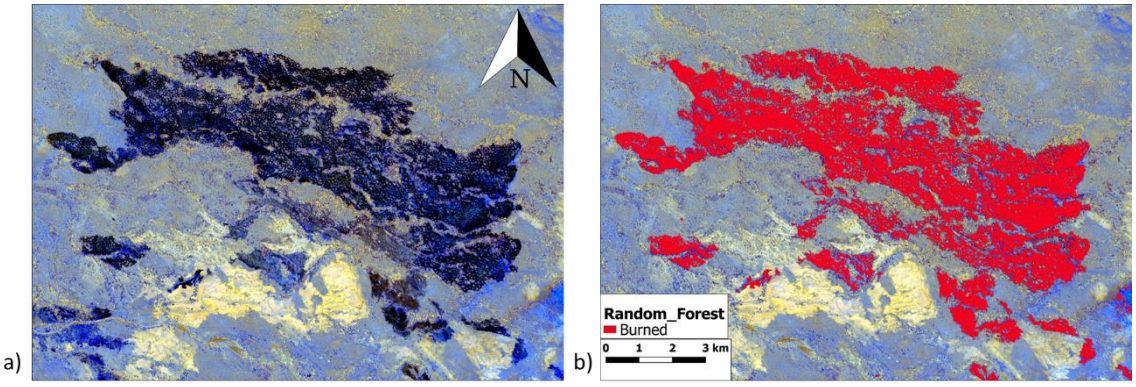

Figure 35: a) Detail of the temporal difference image (RGB: R=NDVI, G=NIR reflectance, B=Red reflectance) between post- and pre-fire dates ($\Delta_{post-pre}$) and b) example of burned area map.

Figure 37 shows example BA maps extracted from Planetscope mosaic images for site 1B (Niokolo_Koba, Senegal) covering the time period January 30th to March 1st, 2019. Since burned areas are derived for temporal difference images, BAs refer to the post-fire date for each pair of mosaic images: 17/01/2019-30/01/2019 (red) and 30/01/2019-

06/03/2019 (orange). RGB false colour image mosaics are shown in Figure 33 (panels a and b).

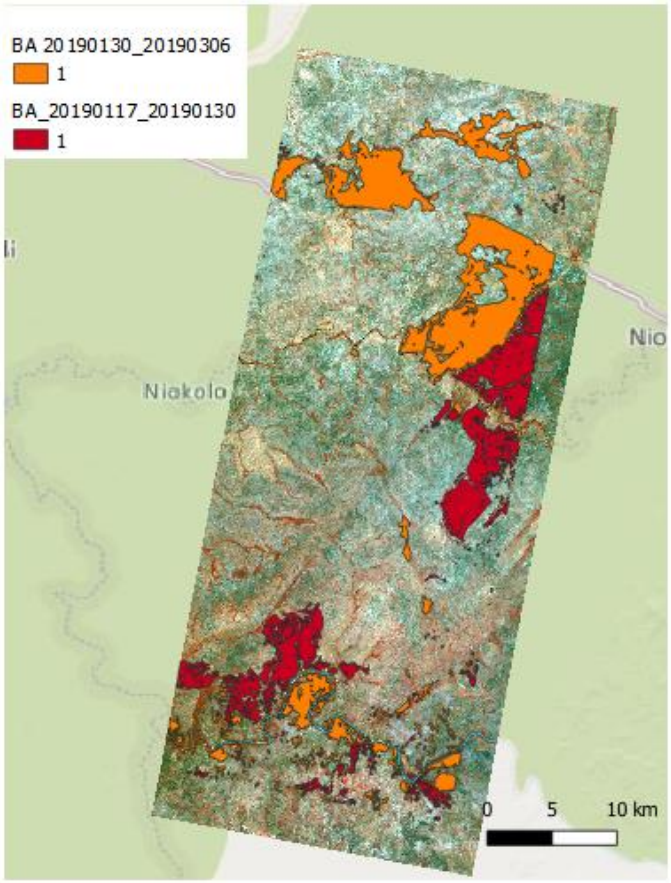

Figure 36: Example classification of burned areas derived from multi-temporal Planetscope mosaic images for site 1B (Niokolo_Koba). On the background, RGB Planetscope image mosaic obtained for 06/03/2019.

2.6 Discussion and conclusions

The protocols for the selection of validation units for accuracy assessment of global and regional/continental Fire_cci BA products were defined and implemented; the source of EO data is Landsat 8 and Sentinel 2, respectively.

L8 validation units for global scale validation were defined based on previous Fire_cci phases (Padilla et al. 2014; 2015); yet some improvements were applied to extend i) the validation region inside each single TSA, i.e. up to an area of 100 km x 100km, and ii) the time period covered by the validation units, i.e. long units vs. short units.

The S2 validation units were instead defined with a new approach based on the S2 tile system used for data archiving and distribution by ESA. The size of the validation units (100 km x 100 km) was set coincident with S2 tiles but some preliminary steps were applied to identify tiles suitable for building the population for subsequent sampling.

The selection of validation units is carried out with a stratified random sampling approach: strata are derived for both validation scales by intersecting Olson biomes and fire intensity layers. The total number of validation units was set to 100 and 50 per year

for global L8 and regional S2 validation, respectively, and the number of units for each stratum was set based on Eq. 2.

Fire reference perimeters were extracted by classification of consecutive L8/S2 scenes over long validation time periods; only L8/S2 scenes with cloud cover lower than 30% were retained and the length of the validation unit (from the start to the end date) is a function of available images, that in turn depends on the biome. The maximum time step between consecutive L8/S2 images was set to 16 days to retain the burned signal. Over the time period covered by the validation unit, only clear-sky pixels are retained for classification into burned/unburned categories. The cumulated cloud cover can significantly affect the cloud free area at the end of the long validation unit available for comparison with the BA product to be validated. A criterion for limiting the cumulated cloud cover over the validation region and long unit is under investigation, in particular for the S2 validation activities.

In this report, preliminary results on accuracy metrics for the FireCCI51 BA product for the year 2018 are presented.

Finally, Planetscope high resolution images (3 m, four spectral bands in the VIS/NIR wavelengths) were analysed for deriving fire reference perimeters for validation of BA products from S2/S1 integration algorithm (FireCCIS1S2AF10).

3 Intercomparison of FireCCI51 with other BA products

The FireCCI51 results of the period 2001-2018 were compared with previous products generated within the Fire_cci project as well as to existing global BA products in Lizundia-Loiola et al. (2020). This section is an adaptation of the results of that analysis. The selected products were the FireCCI41 (derived from MERIS data and available for the period 2005-2011: Chuvieco et al. (2016)), FireCCI50 (based on a previous version of our algorithm: Chuvieco et al. (2018)) and the NASA's MCD64A1 c6 (based on 500m MODIS data: Giglio et al. (2018)). Additionally, with the aim of analysing the sensitivity of each product to small fires the three MODIS products were compared with FireCCISFD11 (at 20m resolution) for Sub-Saharan Africa in 2016 (Roteta et al., 2019). This region was chosen as it covers around 70% of the global BA (Chuvieco et al., 2018; Giglio et al., 2018).

3.1 Intercomparison of spatial and temporal trends among existing products

Temporal trends showed an overall good global agreement between FireCCI51 and NASA MCD64A1 c6 products (Figure 37). FireCCI51 had the highest amount of BA among the compared BA products, with an average annual BA of 4.63 Mkm^2, followed by MCD64A1 c6 with 4.18 Mkm^2 (both for the period 2001–2018) and FireCCI50 with 3.81 Mkm^2 (for the period 2001–2016). FireCCI51 and 50 had less BA in the first two years of the time series, because of partial gaps of MODIS HS caused by being acquired by a single satellite (Terra). After 2003, both Terra and Aqua MODIS data were used to acquire HS, hence the detected amount of BA clearly improved. MCD64A1 c6 was less affected by this issue as some parameters of the algorithm were modified to compensate for the lack of information in those years (Giglio et al., 2018). In any case, temporal trends of FireCCI51 agree with the rest of the BA products, including the peak of 2007 that was missed by FireCCI50.

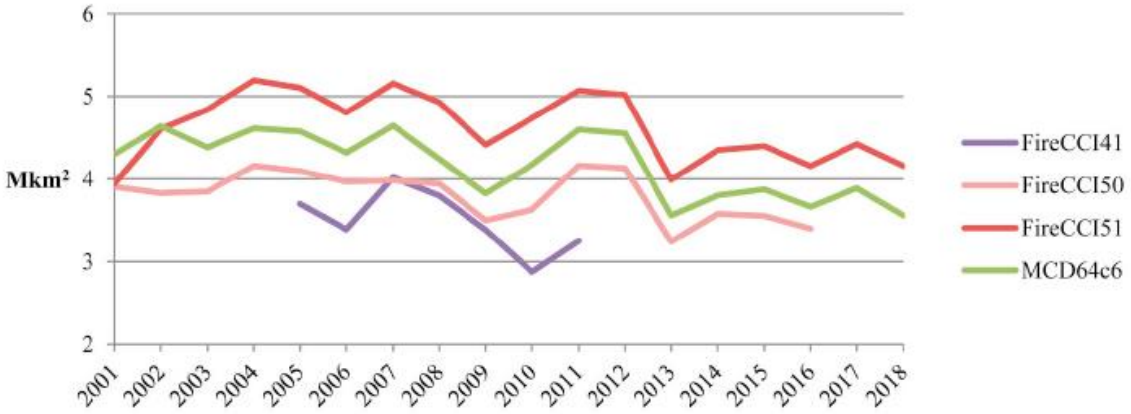

Figure 37: Annual BA of ESA (FireCCI) and NASA (MCD64A1 c6) products

Regarding the spatial patterns, all the products agree in the most affected regions (Figure 38): Northern Hemisphere Africa (NHAF) and Southern Hemisphere Africa (SHAF), although their relative contribution varies from 67.9% (MCD64A1 c6) to 74.6% (FireCCI41). In all cases, SHAF contributes more than the northern region, except for FireCCI41. The second most burned region was Australia (AUST) in all products, although FireCCI41 was less sensitive to this area. FireCCI51 was found more sensitive to boreal fires than other products, having doubled the BA detections than other products, with almost 0.2 Mkm^2 burned annually. A similar pattern was observed in Central Asia (CEAS). Conversely, in Southern Hemisphere South America (SHSA) the MCD64A1 c6 detected 0.03 Mkm^2 more BA than the FireCCI51.

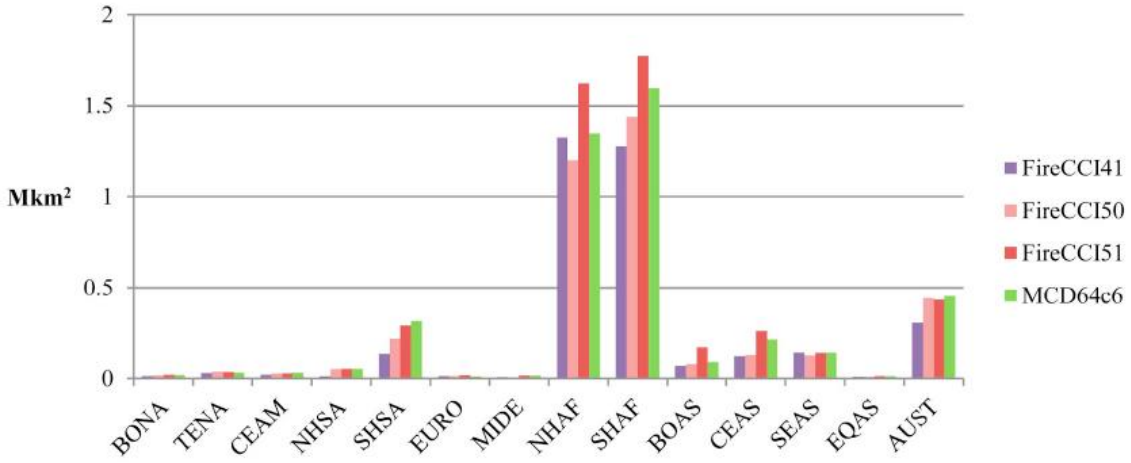

Figure 38: Annual BA average in Mkm2 for each continental region according to FireCCI41, FireCCI50, FireCCI51, and MCD64A1 c6, for the period 2005–2011. Definitions of the regions can be found in Annex 1.

3.2 Sensitivity to small fires detection

FireCCI50 (250 m), FireCCI51 (250 m) and MCD64A1 c6 (500 m) products were spatially compared to the FireCCISFD11 (20 m) product for Sub-Saharan Africa 2016 to analyse the sensitivity of each global product to detecting small fires. The FireCCISFD11 detected 4.9 Mkm^2 for the Sub-Saharan Africa, 60% more than the FireCCI51 (3.1 Mkm^2), 80% more than the MCD64A1 c6 (2.7 Mkm^2), and 97% more than the FireCCI50 (2.5 Mkm^2).

A comparison between the global products and FireCCISFD11 was also performed, taking into account that FireCCISFD11 presents the highest accuracy of all the products, with a DC = 0.77, relB = -0.0896, Ce = 0.193 and Oe = 0.265 (Padilla et al. 2018). Table 10 shows the monthly commission and omission errors of each MODIS product compared to FireCCISFD11. FireCCI51 was observed the most similar product, with an annual DC value of 0.42, followed by the FireCCI50 (DC=0.38) and the MCD64A1 c6 (DC=0.36). During high fire occurrence months, FireCCI51 showed the highest DC values with FireCCISFD11, followed by the FireCCI50 product. For low occurrence months MCD64A1 c6 had similar or slightly higher DC values than the Fire_cci products. The lowest omission error for the FireCCI51 was found in December and June, while the highest was observed in the Spring (March–May). Conversely, the commission error was found lower and much more stable through the year ranging from 41% to 53%.

Table 10: Comission (Ce) and omission (Oe) errors calculated based on the comparison between FireCCISFD11 and the three MODIS BA products for Sub-Saharan Africa in 2016

MONTH	FireCCI50		FireCCI51		MCD64A1 c6	
	Ce	Oe	Ce	Oe	Ce	Oe
January	46.5%	70.8%	49.7%	61.9%	54.1%	68.9%
February	50.0%	83.9%	52.0%	79.5%	60.4%	88.7%
March	45.9%	91.7%	44.6%	89.3%	53.9%	93.3%
April	44.0%	93.8%	47.5%	91.3%	62.0%	88.7%
May	53.4%	75.9%	53.2%	75.1%	59.6%	79.5%
June	49.0%	58.3%	47.0%	56.8%	44.8%	70.3%
July	45.4%	64.5%	45.3%	58.7%	42.9%	69.0%
August	43.5%	74.1%	42.2%	68.2%	42.8%	67.8%
September	47.5%	81.4%	46.5%	66.6%	39.8%	66.5%
October	47.0%	87.1%	41.9%	78.7%	51.1%	73.0%
November	38.2%	69.9%	41.9%	62.0%	43.2%	70.4%
December	42.8%	59.8%	43.8%	56.3%	46.3%	63.9%
Average	**45.4%**	**72.9%**	**45.8%**	**66.5%**	**47.2%**	**71.7%**

A monthly trend between DC and the total amount of BA detected for both hemispheres can be observed in Figure 39. For the NHAF region, FireCCI51 was the most similar product to FireCCISFD11 in most months. MCD64A1 c6 showed a better agreement in low fire occurrence months (April–August) (Figure 39a). For SHAF, a similar trend was observed, with higher DC values for the June–September period (Figure 39b). In both regions, the lowest occurrence months showed also the lowest DC values.

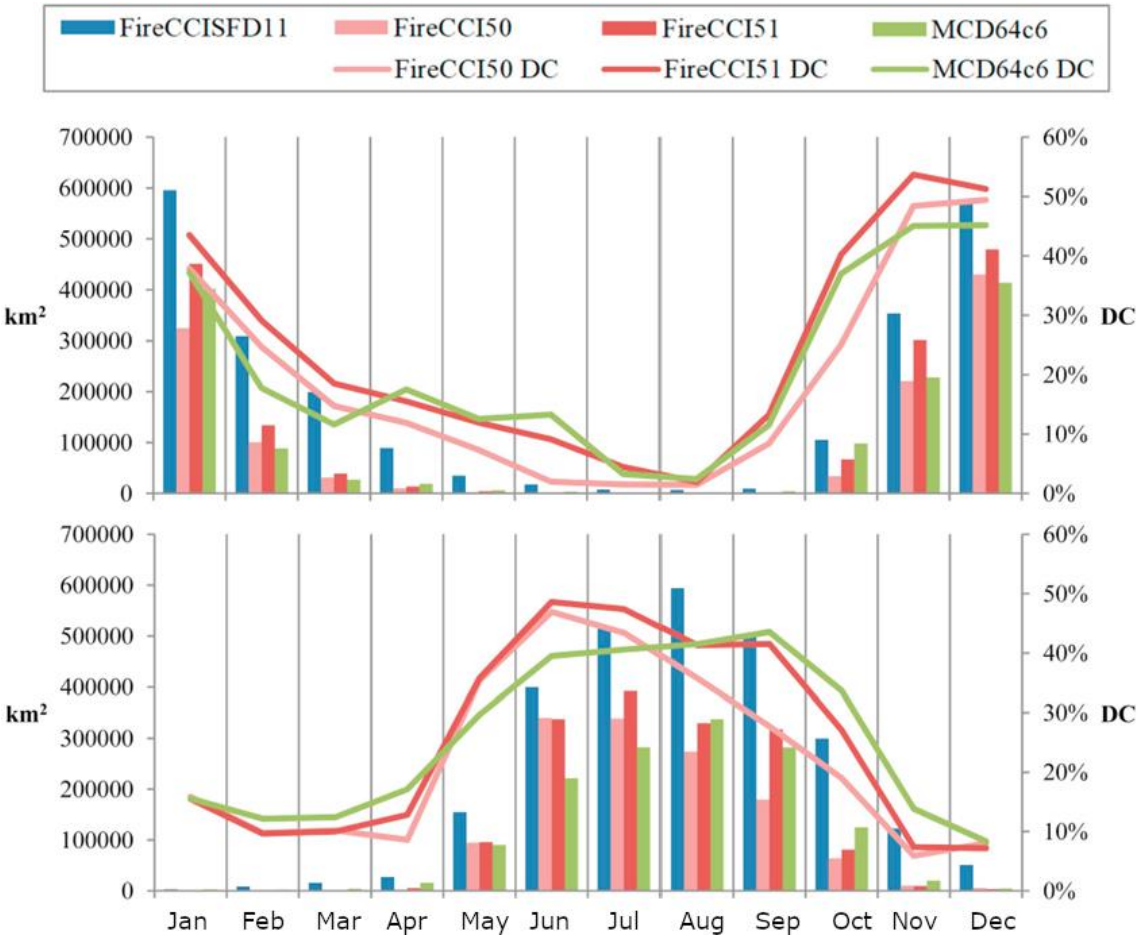

Figure 39: Comparison of the MODIS BA products (FireCCI50, FireCCI51, and MCD64A1 c6) against the Sentinel-2 product (FireCCISFD11) for the year 2016 in Sub-Saharan Africa. a) Northern Hemisphere Africa (NHAF) and b) Southern Hemisphere Africa (SHAF).

4 References

Boschetti, L., Stehman, S., V., & Roy, D.P. (2016). A stratified random sampling design in space and time for regional to global scale burned area product validation Remote Sensing of Environment, 186, 465-478.

Boschetti, L., Roy, D. P., Giglio, L., Huang, H., Zubkova, M., Humber, M. L. (2019) Global validation of the collection 6 MODIS burned area product. Remote Sensing of Environment 235, 111490, https://doi.org/10.1016/j.rse.2019.111490

Chuvieco, E., Lizundia-Loiola, J., Pettinari, M. L., Ramo, R., Padilla, M., Tansey, K., Mouillot, F., Laurent, P., Storm, T., Heil, A., and Plummer, S. (2018). Generation and analysis of a new global burned area product based on MODIS 250 m reflectance bands and thermal anomalies, Earth Syst. Sci. Data, 10, 2015-2031, https://doi.org/10.5194/essd-10-2015-2018.

Chuvieco, E., Yue, C., Heil, A., Mouillot, F., Alonso-Canas, I., Padilla, M., Pereira, J.M., Oom, D., Tansey, K. (2016). A new global burned area product for climate assessment of fire impacts. Glob. Ecol. Biogeogr. 25, 619–629.

Cohen, W.B., Yang, Z., & Kennedy, R.E. (2010). Detecting trends in forest disturbance and recovery using yearly Landsat time series: 2. TimeSync - Tools for calibration and validation. Remote Sensing of Environment, 114, 2911-2924.

Congalton, R.G., & Green, K. (1999). Assessing the Accuracy of Remotely Sensed Data: Principles and Applications. Boca Raton: Lewis Publishers.

Dice, L.R. (1945). Measures of the Amount of Ecologic Association Between Species. Ecology, 26, 297-302.

Giglio, L., Boschetti, L., Roy, D.P., Humber, M.L., Justice, C.O., 2018. The Collection 6 MODIS burned area mapping algorithm and product. Remote Sens. Environ. 217, 72–85.

Kennedy, R.E., Yang, Z., & Cohen, W.B. (2010). Detecting trends in forest disturbance and recovery using yearly Landsat time series: 1. LandTrendr - Temporal segmentation algorithms. Remote Sensing of Environment, 114, 2897-2910.

Key, C. H. & N. C. Benson (1999) The Normalized Burn Ratio, a Landsat TM radiometric index of burn severity. US Geological Survey, Department of the Interior.

Latifovic, R., Olthof, I. (2004). Accuracy assessment using sub-pixel fractional error matrices of global land cover products derived from satellite data. Remote Sensing of Environment, 90, 153-165.

Lemajic, S., Vajsová, B. and Aastrand, P., 2018. New sensors benchmark report on PlanetScope: Geometric benchmarking test for Common Agricultural Policy (CAP) purposes, EUR 29319 EN, Publications Office of the European Union, Luxembourg, 2018, ISBN 978-92-79-92833-8, doi:10.2760/178918, JRC111221.

Lizundia-Loiola, J., Otón, G., Ramo, R. and Chuvieco, E. (2020). A spatio-temporal active-fire clustering approach for global burned area mapping at 250 m from MODIS data. Remote Sensing of Environment, 236, 111493, https://doi.org/10.1016/j.rse.2019.111493.

Moreno-Ruiz, J., García-Lázaro, J.R., Arbelo, M. and Cantón-Garbín, M. (2020). MODIS Sensor Capability to Burned Area Mapping—Assessment of Performance and Improvements Provided by the Latest Standard Products in Boreal Regions. Sensors 2020, 20(18), 5423; https://doi.org/10.3390/s20185423.

Olson, D.M., Dinerstein, E., Wikramanayake, E.D., Burgess, N.D., Powell, G.V.N., Underwood, E.C., D'Amico, J.A., Itoua, I., Strand, H.E., Morrison, J.C., Loucks, C.J., Allnutt, T.F., Ricketts, T.H., Kura, Y., Lamoreux, J.F., Wettengel, W.W., Hedao, P., & Kassem, K.R. (2001). Terrestrial Ecoregions of the World: A New Map of Life on Earth. BioScience, 51, 933-938.

Padilla, M., Stehman, S.V., & Chuvieco, E. (2014). Validation of the 2008 MODIS-MCD45 global burned area product using stratified random sampling. Remote Sensing of Environment, 144, 187-196.

Padilla, M., Stehman, S.V., Ramo, R., Corti, D., Hantson, S., Oliva, P., Alonso, I., Bradley, A., Tansey, K., Mota, B., Pereira, J.M., & Chuvieco, E. (2015). Comparing the Accuracies of Remote Sensing Global Burned Area Products using Stratified Random Sampling and Estimation. Remote Sensing of Environment, 160, 114-121.

Padilla M., Olofsson P., Stehman S.V., Tansey K., Chuvieco E. (2017). Stratification and sample allocation for reference burned area data, Remote Sensing of Environment, 203, 240-255.

Padilla, M., Wheeler, J., Tansey, K. (2018) ESA CCI ECV Fire Disturbance: D4.1.1. Product Validation Report, version 2.1. Available at: https://www.esa-fire-cci.org/documents.

Roteta, E., Bastarrika, A., Padilla, M., Storm, T., Chuvieco, E. (2019). Development of a Sentinel-2 burned area algorithm: Generation of a small fire database for sub-Saharan Africa, Remote Sensing of Environment, 222, 1-17, https://doi.org/10.1016/j.rse.2018.12.011.

Rouse Jr, J. W., R. Haas, J. Schell & D. Deering (1974) Monitoring vegetation systems in the Great Plains with ERTS.

Roy, D. P., P. G. H. Frost, C. O. Justice, T. Landmann, J. L. Le Roux, K. Gumbo, S. Makungwa, K. Dunham, R. Du Toit, K. Mhwandagara, A. Zacarias, B. Tacheba, O. P. Dube, J. M. C. Pereira, P. Mushove, J. T. Morisette, S. K. Santhana Vannan & D. Davies (2005) The Southern Africa Fire Network (SAFNet) regional burned-area product-validation protocol. International Journal of Remote Sensing, 26**,** 4265-4292.

Roy, D. P., H. Huang, L. Boschetti, L. Giglio, L. Yan, H.H. Zhang, Z. Li, (2019) Landsat-8 and Sentinel-2 burned area mapping - A combined sensor multi-temporal change detection approach. Remote Sensing of Environment, 231, 111254, https://doi.org/10.1016/j.rse.2019.111254.

Annex 1: Acronyms and abbreviations

AUST	Australia
BA	Burned Area
BOAS	Boreal Asia
BONA	Boreal North America
CCI	Climate Change Initiative
Ce	Commission error
CEAM	Central America
CEAS	Central Asia
DC	Dice Coefficient
DOY	Day of the Year
ECV	Essential Climate Variables
EO	Earth Observation
EQAS	Equatorial Asia
ESA	European Space Agency
EURO	Europe
FireCCI41	MERIS Fire_cci v4.1
FireCCI50	MODIS Fire_cci v5.0
FireCCI51	MODIS Fire_cci v5.1
FireCCISFD11	Sentinel-2 SFD Fire_cci v1.1
FireCCISFD20	Sentinel-2 SFD Fire_cci v2.0
FireCCIS1S2AF10	Sentinel-1&2 Fire_cci test site in Africa v1.0
GEE	Google Earth Engine
HR	High Resolution
KML	Keyhole Markup Language
L	Validation unit Lenght
L8	Landsat 8
MCD64 c6	MODIS Burned Area product collection 6
MERIS	Medium Resolution Imaging Spectrometer
MIDE	Middle East
MODIS	Moderate Resolution Imaging Spectroradiometer
NASA	National Aeronautics and Space Administration's
NBR	Normalized Burned Ratio
NBR2	Normalized Burned Ratio 2
NDVI	Normalized Difference Vegetation Index
NHAF	Northern Hemisphere Africa
NHSA	Northern Hemisphere South America
NIR	Near InfraRed
NPP	National Polar-orbiting Partnership
Oe	Omission error
PVIR	Product Validation and Intercomparison Report
RF	Random Forest
RGB	Red-Green-Blue composite
S1	Sentinel-1

S2	Sentinel-2
SAR	Synthetic Aperture Radar
SAR-O	SAR-Optical
SE	Standard Error
SEAS	Southern Asia
SFD	Small Fire Database
SHAF	Southern Hemisphere Africa
SHSA	Southern Hemisphere South America
SWIR	Short Wave InfraRed
TENA	Temperate North America
TSA	Thiesen Scene Area
UTM	Universal Transverse Mercator
VHR	Very High Resolution
WGS84	World Geodetic System 1984